2017

Modeling Gas Budgets in Marginal Sea Ice Zones

Arash Bigdeli
University of Rhode Island, arash_bigdeli@uri.edu

MODELING GAS BUDGETS IN MARGINAL SEA ICE ZONES

BY

ARASH BIGDELI

A DISSERTATION SUBMITTED IN PARTIAL FULFILLMENT OF THE

REQUIREMENTS FOR THE DEGREE OF

DOCTOR OF PHILOSOPHY

IN

OCEANOGRAPHY

UNIVERSITY OF RHODE ISLAND

2017

DOCTOR OF PHILOSOPHY DISSERTATION

OF

ARASH BIGDELI

APPROVED:

Dissertation Committee:

Major Professor Brice Loose

Tetsu Hara

M Reza Hashemi

An T Nguyen

Nasser H. Zawia
DEAN OF THE GRADUATE SCHOOL

UNIVERSITY OF RHODE ISLAND
2017

ABSTRACT

Biogeochemical gas budgets at high-latitude regions and sea ice zones are a source of uncertainty in climate models. The four main processes that regulate these budgets include advection, ventilation, mixing, and accumulation/release from sea ice. Considering the scarcity of data in sea ice zones, specifically during winter time, the environment is too poorly sampled to constrain these processes through direct measurements; hence we proposed models to systematically investigate these processes. The models proposed in this dissertation consist of regional numerical ice-ocean models, 1D forward and inversion numerical models, and analytical models.

Manuscript I of this dissertation focuses on a 3D regional Arctic ice-ocean models. The models are based on MIT general circulation model (MITgcm) code. We used 36 km, 9 km and 2 km horizontal resolution of regional MITgcm configuration with fine vertical spacing to evaluate the capability of the model to reproduce the physical parameters that affect the budget. The model outputs of interest from these simulations are sea ice concentration, sea ice speed, water velocities, and mixed layer depth. From gas budget point of view, sea ice concentration and speed effect ventilation, changes in mixed layer depth lead to mixing, and resolving water velocities quantifies the effects of advection.

To assess the accuracy of model, we compared the model outputs to existing field data. We found model sea ice concentration and speed follow data with good fidelity. The model demonstrated the capacity to capture the broad trends in the mixed layer although with a significant bias. We saw improvement in mixed layer depth accuracy

with reducing the horizontal resolution of the model. Finally we showed modeled water velocities have low correlation with point-wise in situ data. This correlation remained low in all three model resolution simulations and we argued that is largely due to the quality of the input atmospheric forcing.

Manuscript II of this dissertation focuses on 1D forward and inversion modeling of gas budgets. Following our results from the first manuscript, we approximated the effects of advection analytically and utilized a 1D model and its inversion code. We applied the model with combination of numerical passive tracers to reproduce the 53 radon profiles gathered in the Arctic. The optimization based on inversion model reduced the uncertainties in initial conditions and supported the 1D model. We showed mixing, if not resolved, can introduce up to 50% error in estimated budgets. When effects of mixing, melt/freeze and advection taken into the account, we show current estimates of gas exchanges under predicts surface flux in almost cover sea ice areas.

Manuscript III presents a new approach in modeling gas exchange in sea ice zones. In this study a sea state dependent gas exchange parametric model is developed based on the turbulent kinetic energy dissipation rate. After comparing this model results with data in the Open Ocean, lakes and marginal ice zones, we applied it to a numerical ice-ocean model of Arctic Ocean. Finally, it is shown that, under the present conditions, gas flux into the Arctic Ocean may be overestimated by 10% if a conventional parameterization is used.

In summary, the work presented in this dissertation evaluates and quantifies the effects of environmental forcing on gas budgets in marginal ice zones and offered insight into main factors regulating near surface gas budgets in marginal sea ice zone.

ACKNOWLEDGMENTS

Firstly, I would like to express my sincere gratitude to my advisor Prof. Brice Loose for the continuous support of my Ph.D study and related research, his patience, motivation, and immense knowledge. His guidance helped me in all the time of research and writing of this thesis. I could not have imagined having a better advisor and mentor for my studies.

Besides my advisor, I would like to thank the rest of my thesis committee: Prof. Tetsu Hara, Prof. An T Nguyen, and Prof. M. Reza Hashemi, for their insightful comments and encouragement, but also for the hard question which incented me to widen my research from various perspectives.

I would like to thank love of my life, my insightful wife Fatemeh Faghihzadeh for all her support and standing by me in good times and bad. Although he was not still born during my defense, I want to thank god for having my son, little Liam in my life who shined a new light in our life. I also want to thank my father who was the biggest support in all stages of my life, may he rest in peace.

My sincere thanks also goes to Physical Oceanography Group specifically Prof. Peter Cornillon, Prof. Kathleen Donohue, Prof. Isaac Ginis at Graduate School of Oceanography, Prof. Stephan Grilli, Prof. Stephen Licht and Prof. Jason Dahl at the Ocean Engineering Department, who provided me an opportunity to learn and improve my research skills.

I thank my fellow colleague Mohammad Reza Abtahi for the stimulating discussions, his invaluable helps, and for all the fun we have had in the last four years.

Last but not the least, I want to say thank you to all my dear friends, specially Amir Banari, Soroush Kouhi, Fatemeh Nemati, Elmira Shekari, Armin Sadighi, Arash Shirazi, Amir Shirazi, Shaghayegh Rezazadeh, Anita Tolouei, Victoria Treadway, Steven Koch and Sam Gratzman.

PREFACE

This dissertation was prepared according to University of Rhode Island 'Guidelines for the Format of Thesis and Dissertation" standards for Manuscript format. This dissertation consists of three manuscripts that have been combined to satisfy the requirements of the Graduate School of Oceanography, University of Rhode Island.

MANUSCRIPT I: Numerical investigation of the Arctic ice-ocean boundary layer; implications for air-sea gas fluxes

This manuscript has been published in peer-reviewed journal "Ocean Sciences", Jan 2017.

MANUSCRIPT II: Forward and inverse modeling of near surface gas budgets in marginal ice zones, from gas exchange to mixing

This manuscript has been prepared for publication and will be submitted to "Global Biogeochemical Cycles"

MANUSCRIPT III: Wave attenuation and gas exchange velocity in marginal sea ice zone

This manuscript is under peer review in "Journal of Geophysical Research"

TABLE OF CONTENTS

LIST OF FIGURES

FIGURE PAGE

Manuscript I

Manuscript II

Manuscript III

Manuscript I

Numerical investigation of the Arctic ice-ocean boundary layer; implications for air-sea gas fluxes

A. Bigdeli[1], B. Loose[1],An T Nguyen[2], S. T. Cole[3]

Published at Ocean Science Journal (2017)

[1]Graduate School of Oceanography, University of Rhode Island, Rhode Island, 02882, U.S.A

[2]University of Texas at Austin, Austin, Texas, 78712, US

[3]Woods Hole Oceanographic Institution, Woods Hole, Massachusetts, 02543, U.S.A

Correspondence to: A.Bigdeli (Arash_Bigdeli@uri.edu)

Abstract. In ice-covered regions it is challenging to determine constituent budgets – for heat and momentum, but also for biologically and climatically active gases like carbon dioxide and methane. The harsh environment and relative data scarcity make it difficult to characterize even the physical properties of the ocean surface. Here, we sought to evaluate if numerical model output helps us to better estimate the physical forcing that drives the air-sea gas exchange rate (k) in sea ice zones. We used the budget of radioactive ^{222}Rn in the mixed layer to illustrate the effect that sea ice forcing has on gas budgets and air-sea gas exchange. Appropriate constraint of the ^{222}Rn budget requires estimates of sea ice velocity, concentration, mixed layer depth, and water velocities, as well as their evolution in time and space along the Lagrangian drift track of a mixed layer water parcel. We used 36 km, 9 km and 2 km horizontal resolution of regional MITgcm configuration with fine vertical spacing to evaluate the capability of the model to reproduce these parameters. We then compared the model results to existing field data including satellite, moorings and Ice-tethered profilers. We found that mode sea-ice coverage agrees with satellite-derived observation 88 to 98% of the time when averaged over the Beaufort Gyre, and model sea-ice speeds have 82% correlation with observations. The model demonstrated the capacity to capture the broad trends in the mixed layer although with a significant bias. Model water velocities showed only 29% correlation with point-wise in situ data. This correlation remained low in all three model resolution simulations and we argued that

is largely due to the quality of the input atmospheric forcing. Overall, we found that even the coarse resolution model can make a modest contribute to gas exchange parameterization, by resolving the time variation of parameters that drive the ^{222}Rn budget, including rate of mixed layer change and sea ice forcings.

1 Introduction

The ocean surface is a dynamic region where momentum, heat and salt, as well as biogeochemical compounds are exchanged with the atmosphere and with the deep ocean. At the sea-air interface, gases of biogenic origin and geochemical significance are exchanged with the atmosphere. Theory indicates that the aqueous viscous sublayer, which has a length scale of 20 to 200 μm (Jähne and Haubecker 1998), is the primary bottleneck for air-water exchange. Limitations in measurement at this critical scale have led to approximations of sea-air gas exchange based on indirect measurements. Four approaches involving data are typically used (Bender et al. 2011), 1) Parametrization of the turbulent kinetic energy (TKE) at the base of the viscous sublayer 2) Tracing purposefully injected gases (Ho et al. 2006; Nightingale et al. 2000a) 3) Micro Meteorological methods (H. J. Zemmelink et al. 2006a; Zemmelink et al. 2008; Blomquist et al. 2010; Salter et al. 2011), and 4) Radon-deficit Method. Here, we examine the radon-deficit method (4), together with a parameterization of the TKE forcing (1) that theoretically leads to the observed deficit in mixed-layer radon.

When the ocean surface is not restricted by fetch, TKE is mostly dominated by wind speed and waves (Wanninkhof 1992; H. J. Zemmelink et al. 2006b; Wanninkhof and

McGillis 1999; Nightingale et al. 2000b; Sweeney et al. 2007; Takahashi et al. 2009). In the polar oceans wind energy and atmospheric forcing are transferred in a more complex manner as a result of sea ice cover (Loose et al. 2009, 2014; Legge et al. 2015). Sea ice drift due to Ekman flow (McPhee and Martinson 1992), freezing and melting of ice leads on the surface ocean (Morison et al. 1992) and short period waves (Wadhams et al. 1986; Kohout and Meylan 2008) all constitute important sources of momentum transfer. Considering the scarcity of data on marginally covered sea-ice zones (Johnson et al. 2007; Gerdes and KöBerle 2007), especially during Arctic winter time, the environment is too poorly sampled to constrain these processes through direct measurement or empirical relationships.

Lacking sufficient data to constrain these processes, we wonder whether it is possible for a numerical model to adequately capture forcing of air-sea gas exchange in the sea ice zone and consequently improve predictions of air-sea flux. The parameters of interest are sea ice concentration (or fraction of open water), sea ice velocity, mixed layer depth, and water current speed and direction in the ice-ocean boundary layer (IOBL) (Loose et al. 2014). Here we use the budget of ^{222}Rn gas in the IOBL as an example, because the radon-deficit method has emerged as one of the principle methods to estimate gas exchange velocity in ice-covered waters (Rutgers Van Der Loeff et al. 2014; Loose et al. 2016).

The Radon deficit method involves sampling ^{222}Rn and ^{226}Ra in the mixed layer to examine any difference in the concentration or (radio) activity of the two species. Radon is a gas, radium is a cation; in absence of gas exchange ^{222}Rn and ^{226}Ra enter secular equilibrium meaning the amount of ^{222}Rn produced is equal to decay rate of

^{226}Ra. Any missing ^{222}Rn in the mixed layer is attributed to exchange with atmosphere (Peng et al. 1979).

Since the ^{222}Rn concentration in air is very low, less than 5% (Smethie et al. 1985) and considering that concentration is proportional to activity/decay rate A, we can use Eq. (1) to determine gas exchange. Where k gas transfer velocity in (m d^{-1}), A_E is the activity or decay rate of ^{222}Rn which in secular equilibrium is equal to ^{226}Ra activity, A_M is ^{222}Rn measured decay rate in mixed layer, λ is decay constant of ^{222}Rn (0.181 d^{-1}) and h is the mixed layer depth

$$k = \left[A_E/A_M - 1\right]\lambda\, h \qquad (1)$$

The mixed layer depth, h, is calculated from the measurements performed at the hydrographic stations during ^{222}Rn sampling process. Gas transfer velocities from equation (1) reflect the memory of ^{222}Rn for a period of two to four weeks (Bender et al. 2011), which is four to eight times the half-life of ^{222}Rn (3.8 days).

This memory integrates the physical oceanography properties of the IOBL, including sea ice cover, mixed layer depth and water current speed. These processes are likely to vary significantly during this period and it is important to consider them as a source of uncertainty in Eq. (1). To illustrate this uncertainty, consider a mixed layer that rapidly changes by a factor of 2 just prior to sampling for radon. If the mixed-layer becomes shallower by stratification, h will be smaller by factor of 0.5 while A_E/A_M in the mixed layer remains the same. Based on equation 1, this causes k to be half of its true value. That is, prior to stratification TKE forcing was sufficient to ventilate the ocean to a depth greater than the apparent h (Bender et al. 2011).

Conversely, if the mixed layer deepens due to mixing, h increases and a new parcel of water with $A_E/A_M = 1$ is added to mixed layer, causing the activity ratio to come closer to unity. These two influences on equation 1 (increasing H and A_E/A_M approaching unity) work against each other, but the net effect is to cause k to appear larger. The change of factor of 2 or higher (in case of convection) in mixed layer depth in less than two weeks has been observed during several studies (Acreman and Jeffery 2007; Ohno et al. 2008; Kara 2003).

The "memory" of gas exchange forcing that radon experiences is further complicated by the presence of sea ice. Consider two alternate water parcel drift paths that lead to the ^{222}Rn sampling station in sea-ice zone (Figure 1). Path B demonstrates a history in which water column spends most its back trajectory under sea-ice. Path "A" shows a water column which experiences stratification and shoaling of mixed layer depth equal to δh when drifting through a region that is completely uncovered by ice. During most of Path "B" gas transfer happens in form of diffusion through sea-ice and it will have a very low k (Crabeck et al. 2014; Loose et al. 2011), in contrast Path "A" will have a greater radon deficit, but a smaller h because of stratification. In either case, it is critical to take into account the time history of gas exchange forcing, including changes in the mixed-layer and ice cover, which has led to the apparent radon deficit at the time of measurement.

This observation about drift paths in the sea ice zone strongly implies that we must consider both time and space in estimating the forcing conditions that are recorded in the radon deficit. In other words, we require a Lagrangian back trajectory of water

parcels to track the evolution of mixed layer and its relative velocity 4 weeks prior to sampling.

Although satellite data, Ice tethered drifters (Krishfield et al. 2008) and moorings (Krishfield et al. 2014; Proshutinsky et al. 2009) have provided valuable seasonal and spatial information about the sea ice zone, they do not track individual water parcels and tend to convolve space and time variations. The spatial limitation of these data poses a challenge to producing a back trajectory of the water parcel.

To address the above mentioned challenges, we use a suite of the Estimation of the Circulation and Climate of the Ocean (ECCO) project's Arctic regional configurations to test the if a numerical model can be used to follow the back trajectory of a radon-labelled water parcel and the gas exchange forcing acting upon it and yield the missing information required for the Radon deficit method.

The variables and derived quantities of interest from the numerical model include mixed layer depth (MLD), sea ice concentration and speed (Loose et al. 2014) and the water velocity in the MLD. We note that as part of the Arctic Ocean Model Intercomparison Project (AOMIP), a number of Arctic ocean-ice models' capability to represent the main ice-ocean dynamics have been assessed (Proshutinsky et al. 2001; Lindsay and Rothrock 1995, p. 995; Proshutinsky et al. 2008). Our reasons for choosing ECCO over other Arctic models stem from the higher correlation between the ECCO's regional Arctic simulated outputs to satellite derived sea ice data (Johnson et al. 2012) and the feasibility in the MITgcm to adapt a high near surface vertical resolution to existing configurations.

The remainder of the article is organized as follows: In section 2 we provide the details of the ECCO ice-ocean models. Section 3.1 and 3.2 focus on model outputs of sea-ice concentration and velocity and comparison with observations from satellite and Ice tethered profilers. Section 3.3 investigates the modeled output salinity and temperature structure and the resulting upper ocean density structure and mixed layer. Section 3.4 evaluates the correlation in near surface water velocity. In section 4 we discuss the results and sources of error and their impact on estimated gas exchange and lastly, section 5 provides the summary of our results.

2 Method

2.1 ECCO model configurations

Three ECCO configurations are used, at horizontal grid spacings of 36 km, 9 km, and 2 km, respectively. The models are based on the Massachusetts Institute of Technology general circulation model (MITgcm) code and employ the z coordinate system described in Adcroft and Campin (2004). Our approach is first to assess the model outputs from the coarse resolution model using model-data misfits, then to investigate if there is quantitative reduction in model-data misfits with higher horizontal resolutions. Surface forcings are from the 25 year Japanese Reanalysis Project (JRA25)(Onogi et al. 2007) for 36 km and 9 km runs and the European Centre for Medium-Range Weather Forecasts (ECMWF) analysis for 2 km run. Initial conditions are from World Ocean Atlas 2005 (Antonov et al.; Locarnini et al.) and initial sea ice conditions are from (Zhang and Rothrock 2003) for the of 36 and 9 km, from which the models are allowed to spin up from 1992. The 2 km global run is

initialized from a 4 km spin up version of the ECCO adjoint-based state-estimate for Jan 2011 and covers the period Feb 2011 to Oct 2012. The vertical mixing uses K profile parameterization (KPP) developed by (Large et al. 1994) and 36 and 9 km runs utilize salt plume parameterization of Nguyen et. al(2009). The horizontal boundary condition for the 36 km and 9 km configurations comes from existing global ECCO2 model outputs (Marshall et al. 1997; Menemenlis et al. 2008; Losch et al. 2010; Heimbach et al. 2010).

We introduced a set of new vertical grid spacings to allow us to capture near surface small details which cannot be represented with the coarser grid system. In the 36 km (hereafter referred to as A1) and 9 km (called A2) models, the spacing is 2 m in the upper 50 m of the water column and gradually increases to a maximum of 650 meters. In contrast, the 2 km model (called A3) has 25 layers in the top 100 meters of water column, starting from 1 meter and increasing to 15 meters step. All the boundary conditions from ECCO2 have been interpolated to match the new vertical grid system.

2.2 Observations

Satellite-derived estimation of sea-ice cover at 25km horizontal resolution (Comiso 2000) is interpolated to a horizontal grid system to facilitate model-data comparison. In addition, sea-ice drift gathered by 28 Ice Tethered Profilers (ITP) (Krishfield et al. 2008) which have more than 2 months of data in Beaufort Sea between 2006 and 2013 have been used to do the ice velocity comparison.

We compared near surface water velocity data from Ice Tethered Profiler with Velocity instruments (ITP-V) (Williams et al. 2010) to A1 and A2 and upward looking

Acoustic Doppler Current Profiler installed on McLane Moored Profiler (MMP) (McPhee et al. 2009; Cole et al. 2014) to A1, A2 and A3 in order to compute the accuracy and feasibility of calculating back trajectory of parcels located in the mixed layer. We limit our comparison of ITP-V which runs from Oct-2009 to Mar-2010 to A1 and A2 since those models run from 2006 to 2013 and A3 runs from 2011 to 2013.

Using salinity and temperature profiles from ITPs (Krishfield et al. 2008) we calculated mixed layer depth and compared it to 2m vertical resolution model output (A1,A2). Most of the observed data exist in Beaufort Gyre, hence we mostly focus our comparison to that geographic perimeter. Figure 2 depicts the bathymetry and location of most important observations we used to make the comparisons with the model.

3 Results

3.1 Sea ice concentration

For Sea ice concentration analysis we introduced a grid system covering the Beaufort Gyre and interpolated the data from satellite (Comiso 2008) and A1 on to the grid. The analysis grid extends from 70° to 80° north and 130° to 170° west, covering most of Beaufort Gyre (Figure 3). Grid points can be divided into two main geographic zones that are marked out based on sea ice cover. The first zone contains grid points where the annual average sea ice cover is greater than 80%. These sets of points are fully covered by sea-ice most of the year. The second zone can be described as “marginally ice covered” wherein the ocean surface is free of ice for some fraction of the year. We chose 3 points within this sea ice geography to compare the seasonal and interannual

behavior of the model with satellite ice cover. The points are located at 80° N,131.82° W (P1), 70.82° N 169.82° W(P2), and 74.76° N and 163.51° W (P3).

The ice cover at P1, P2 and P3 (Figure 3) can be divided into 3 ice phases: (a) Fully covered in ice, (b) Open water and (c) a transition between (a) and (b). P3, which is the furthest south, has all three phases. In contrast P1 ice cover only dips below 60% for two brief periods during the 7 year time series depicted in Figure 3 - once in 2008 and again in 2012. These three points illustrate where and when the model has the greatest challenge reproducing the actual sea ice cover. At the extremities of the ice pack, where the water is predominantly covered by 100% or 0% ice (P1 and P3), the model captures the seasonal advance and retreat and the percent ice cover itself is accurate. However, in the transition regions that are characterized by marginal ice for much of the year (P2), the model has more difficulty reproducing the observed sea ice cover as well as the timing of the advance and retreat. This behavior is consistent with the description that has been explained by Johnson et al. (2007), that models have a higher accuracy predicting sea ice concentration in central Arctic and less accuracy near periphery and lower latitudes.

The spatial sensitivity of the model can be observed using root mean square (RMS) error (Hyndman and Koehler 2006) Eq. (2), calculated over the 1992-2013 period (Figure 3). The area with the highest misfits coincides with area between the 80% and 60% contour lines (Figure 3) and is concentrated primarily in the Western Beaufort. The RMSE error of 0.2 is the maximum value away from land, this same level of error can also be found near land which is caused by fast-ice generation. Fast Ice in the

model is replaced with pack of drifting sea ice; this error is common among numerical models and has been brought to attention during AOMIP (Johnson et al. 2012).

$$\mathrm{RMSE}\ (\mathrm{point}\ ) = \sqrt{\sum_{i=1}^{n} (C_{\mathrm{simulation}} - C_{\mathrm{satellite}})^2 / n} \qquad (2)$$

If we compare the monthly climatology for sea ice cover over the 1992-2013 period, the RMS error between model and satellite data is least during the early winter months (e.g. Jan-Mar) when sea ice is close to its maximum extent. Comparing Data and A1 Figure 3 depicts an increase in RMSE during July, August, September and October and a minor decrease in May and November. The RMSE appears to be greater during the summer months of ice retreat, and slightly less during the autumn months of ice advance. Overall, the periods of transition (melt and freeze) coincide with the greatest RMSE.

An important source of errors in the model ice concentration comes from the reanalysis surface forcing. Fenty and Heimbach (2012) showed that adjustments in the air temperature that are within the uncertainties of this reanalysis field can help bring the model ice edge into agreement with the observations. Of note also is that the uncertainty in satellite-derived ice cover can be the highest in the marginal ice zone due to tracking algorithms that are sensitive to cloud liquid water or cannot distinguish thin ice from open water (Ivanova et al. 2015), this error also manifests itself in quantification of model-data misfits.

3.2 Sea ice velocity

Ekman turning causes ice and water to move at divergent angles with respect to each other. Ice moves the fastest, with mean values of 0.09 m s^{-1} (Cole et al. 2014), and the water column progressively winds down in velocity, along the Ekman spiral. Stratification in the Arctic leads to a confinement of the shear stress closer to the air-sea interface and also produces greater divergent flow vectors between ice and water (McPhee 2012). In the marginal ice zone or in regions where ice is converging or diverging, these motions, relative to the motion of the water column can produce significant changes in the water column momentum budget as well as air-sea fluxes. Thankfully, the ITPs can provide us with a measure of the real ice drift.

To generate a more quantitative comparison between the results we utilized the same method introduced by Timmermans et al. (2011), to compare ice velocity components (eastward - northward) of A1 to ITP velocity and compute the correlation coefficient of each experiment with the daily averaged actual drift velocity from the ITPs (Figure 4).

When averaged over all the ITPs operating in Beaufort Gyre during 2006 to 2013, A1 had correlations of 0.8 with actual velocity components and 0.82 correlation with speed magnitude. RMSE calculated for A1 based on Eq. (2) shows an error of 0.043 ms^{-1} and no significant bias.

3.3 Temperature, salinity, density and MLD

3.3.1 Vertical Salinity and Temperature profiles

We chose 4 hydrographic profiles in the Beaufort Sea to assess the simulated vertical salinity and temperature. The first two sets of profiles are from ITP-1 winter and

summer 2006; the third set is from ITP-43 during winter 2010 and the fourth is from ITP-13 during summer 2008 (Figure 5). For visualization we linearly extrapolated the profiles from the first layer of the model up to the surface, which occurs over the top 1 meter of the water column.

During winter time, the model Temperature and Salinity profiles show a well mixed layer that extends below 15 meters, followed by a very large gradient. The mixed-layer temperature is close to the local freezing point in a condition called “ice bath” (Shaw et al. 2009). The ITP profiles are similar; however the ITP mixed layer depth is deeper by nearly 10 meters, indicating more ice formation and convective heat loss over this water column, as compared to the model water column. In summer the model mixed layer shoals to approximately 5 meters depth following two local temperature extrema, the bigger maximum is at ~35 meters generated by intrusion of the Pacific Summer Water (PSW) which is a dominant feature in Canada basin. The second smaller maximum happens around 10 meters called Summer Mixed Layer (Shimada et al. 2001, p. 201) or Near-Surface Temperature Maximum (NSTM) (Jackson et al. 2010) which is a seasonal feature generated by shortwave solar heat diffusion (Perovich and Maykut 1990). These two well-defined phenomena are broadly descriptive of the summer surface layer in the Beaufort Gyre. They are; however, absent from the ITP data at this location, indicating a different ice and heat budget time history.

Data and model profiles in Figure 5b show better agreement in the shape and the absolute value of the T and S profiles. Both model and ITP data have a 20 meter deep mixed layer during 2010 winter. The model in this case does not show as much change

in vertical temperature structure compared to actual data. In the profile from ITP-13 (Figure 5) the model again over estimates the temperature beneath the mixed layer, although certain features including the NSTM can still be found near 10 meters, yet not as pronounced since it is very close to PSW. Bearing in mind that density in the Arctic is dominated by changes in salinity, we move forward to density profiles from this point on.

In addition, we note that recent studies show that eddies with diameters of 30 km or less (Nguyen et al. 2012; Spall et al. 2008; Zhao et al. 2014; Zhao and Timmermans 2015; Zhao et al. 2016) play an important role in transporting Pacific water from the shelf break into Canadian basin. Adequate representation of ocean eddies and investigation their roles in setting the water column stratification require a model with finer horizontal resolution. Hence moving forward, in addition of A1, we utilize the 9km model (A2) to investigate the density profiles as well as study the MLD.

3.3.2 Density profiles

We compared the 36 km and 9 km model outputs of density to the time series of density profiles from ITP-35 (Figure 6) starting in Oct 2009 to Mar 2010. A black mask indicates locations where there is no data from ITP-35 - particularly in the upper 7 meters of the water column. As ITP-35 transited through Canadian basin, density profiles contain both temporal and spatial changes.

We are able to discern some broad similarities between the model and ITP density profiles. From November through January, both ITP and model density profiles remain relatively constant. Between February and March, ITP-35 appears to drift

through a zone of convection, likely caused by ice formation, with sudden increase of density near the surface. The same feature can be observed in both A1 and A2 density. However, on a smaller scale, there is significantly more variation in the ITP data than what the model represents.

For exploring the reason behind the density signals, we used the simulated fraction of sea ice cover and ice thickness (Figure 6). The dominating effect appears to result from sea ice fraction when there is almost continuously covered area. The changes from sea ice thickness can be observed in the volume of fresh water in the water column, as seen by outcropping of the 1022.5 isopycnal coinciding with the increase of sea ice thickness. An increase in near surface density can be seen in late January and early February accompanied by an increase in ice thickness and insertion of brine in the water column. The second peak, which is not as pronounced, happens in late February when ice fraction decreases from 100% to 95% and exposes the surface water to cold atmosphere, leading to production of newly formed sea ice. We further examine these signals in MLD section below.

3.3.3 Mixed layer depth

There are many different methods in the literature for calculating mixed layer depth (Brainerd and Gregg 1995; Wijesekera and Gregg 1996; Thomson and Fine 2003; de Boyer Montégut et al. 2004; Lorbacher et al. 2006; Shaw et al. 2009). The methods can be divided into two main types (Dong et al. 2008): The first type of algorithm looks for the depth (z_{MLD}) at which there has been a density increase of $\delta\rho$ between the ocean surface and z_{MLD}. A typical range of values for $\delta\rho$ are 0.005 (kg m^{-3}) to 0.125

(kg m^{-3}) (Brainerd and Gregg 1995; de Boyer Montégut et al. 2004). The second type uses slightly different criteria, where the base of the mixed layer is determined as the depth where the gradient of density ($\partial\rho/\partial z$) equals or exceeds a threshold; typical numbers for ($\partial\rho/\partial z$) are 0.005 (kg m^{-4}) to 0.05 (kg m^{-4}) (Brainerd and Gregg 1995; Lorbacher et al. 2006, p. 200). A more sophisticated approach to type 1 of these criteria is to utilize a differential between (ρ_{100m} - $\rho_{surface}$) as the cut of point (instead of using a fixed $\delta\rho$) to account for the effects of surface ρ changes during winter and summer (Shaw et al. 2009). Here, we have implemented two of these methods M1 and M2, with M1 using $\delta\rho$ equal to 0.2 of (ρ_{100m}–$\rho_{surface}$) (Shaw et al. 2009) and M2 with a gradient ($\partial\rho/\partial z$) cut off point equal to 0.02 (kg m^{-4}) which matches innate model parametrization of MLD (Nguyen et al. 2009).

We compare these 2 methods by applying them to the profiles from Figure 5 and the results are shown in Figure 7. In case (a) and (b) M1 produces a mixed layer depth that is 8 to 12 meters deeper, compared to the other method. A visual examination of profiles indicates that the M1 criteria may be too flexible of a criteria. The results from M1 appear to be intermittently "realistic", whereas M2 can be difficult to implement for data sampled at high vertical resolution as a result of greater small-scale variability. In practice, we find M1 is the most straight-forward to implement.

It should be mentioned that it is difficult to consistently compare performance of the M1($\delta\rho$) and M2 methods on ITP and model data, because the model data extends to top 1 m of water column, whereas the ITP data stops at 7 m depth (Peralta-Ferriz and Woodgate 2015). Furthermore, it has been shown that summer mixed layer in the Canada basin can be less than 12 meters (Toole et al. 2010). To account for this effect,

we apply an additional restriction wherein any profile whose mixed-layer depth is less than 2 m below the shallowest ITP measurement is discarded. This restriction effectively removes any ML depths shallower than 10 meters due to ITP sampler not resolving the upper 8 m of water column. In some cases, a remnant mixed-layer from the previous winter may exist in the water column. In this case, the methods incorrectly identify the remnant ML as actual ML depth.

To compare the methods over a longer time period, we calculated the mixed-layer depth from model data and ITP-35 data along the ITP-35 drift track. We used M1 to determine the ML depth for A1, A2 and for ITP-35 data (Figure 8). Both model results show a shallower ML compared to the ITP data; the most prominent feature in late January corresponds to a sudden change in density found in (Figure 6). Beside the above mentioned peak A1 fails to capture any variability in MLD whereas A2 shows that ML deepens by about 10 meters in mid February corresponding to ice opening occurring during the same time span (Figure 6). The difference between A1 and A2 and their ability to capture MLD change, can be explained by the capability of a higher resolution model to capture small-scale fractures in the ice cover (Figure 8), and conversely, the inability of the coarser resolution to do so is due to averaging over a larger grid. The wind appears to be the primary driving mechanism for the divergence in ice cover, which in turn exposes the ocean to the cold atmosphere and leads to a loss of buoyancy and an increase in MLD. With higher resolution these openings can be captured, leading to a better agreement with data in marginal ice zones. The changes in MLD are of first-order importance to the calculation of gas budgets such as the radon deficit. In this regard a fine-scale grid resolution has real

advantages through its ability to capture both the ice advection and openings in ice cover that lead to MLD change. Coarser resolution would be justified when the point of interest is sufficiently far away from leads and marginal ice zones where the effect of sea-ice dynamics on MLD is important, so the effects of area averaging would be small enough to omit.

One last important note is the effect of the salt plume parameterization (SPP) on MLD. Nguyen et al. (2009) demonstrated the need to remove the artificial excessive vertical mixing in coarse horizontal resolution models. To rule out the dependency of this parametrization to vertical resolution as a source in MLD bias, we performed a suite of 1D tests, with and without the SPP on a variety of vertical resolutions (not shown here) and sea ice melting/freezing scenarios and confirmed that SPP is not dependent on vertical grid spacing. We also investigated MLD in A3 (no SPP) run compared to A2, and confirmed the average MLD is the same between these 2 runs.

3.4 Velocities in the water column

We have very little information from direct observations that permit us to track a water parcel especially beneath sea ice. This is one area where model output could be critical as there are not obvious alternatives. To assess the consistency of the model water current field, we compared 2D model water velocity to data gathered from two sources: (1) from ADCPs mounted on moorings that were deployed starting in 2008 in Beaufort Gyre (Proshutinsky et al. 2009) and (2) the ITP-V sensor equipped with MAVS (Modular Acoustic Velocity Sensors) (Williams et al. 2010), which was the only operating ITP before 2013 which had an acoustic sensor mounted on it.

We compared the velocity components averaged from 5 m to 50 m to account for flow direction that is moving the water parcels in the mixed layer over the duration of ITP-V working days which is from Oct 9, 2009 to Mar 31, 2010 (Figure 9). The ITP data has been daily averaged to remove higher frequency information which we do not expect the model to capture due to the low frequency (6-hourly) wind forcing. Both A1 and A2 show less than 0.3 correlations with data with no improvement in respect to resolution.

We further add A3 to our comparison for moorings velocities (Figure 9), and compared velocities at 25m, which is the level that is shared between all our models and removes the necessity of any interpolation. The simulation results show RMSE normalized by data of higher than 5 and correlations of less than 0.3 over 3 moorings and almost two years of data. This result indicates ocean currents are not well captured in the model irrespective of horizontal grid resolution. We must therefore look into the atmospheric forcing as a likely source of error on high frequency water velocities near surface. As noted above, the wind inputs into the model from the reanalyses are available at a 6-hourly frequency. Chaudhuri et al. (2014) and Lindsay et al. (2014) have compared various available reanalysis products over the Arctic which we used to force our model, along with multiple other reanalysis products with available ship-based and weather station data and found out that wind products in all of those have low correlation i.e less than 0.2. To investigate we compared JRA55 (Onogi et al. 2007) and NCEP (Kalnay et al. 1996) to a shipboard data gathered during 2014 in time span of 2 months in Arctic and found that JRA55 had -0.20 correlation, RMSE of 7.36 and bias of -1.3, NCEP had correlation of 0.10, RMSE of 5.73 and bias of -1.40 when

compared with high frequency data on each cruise, reinforcing our suspicion of high frequency wind as a source of error in water currents.

4 Gas exchange estimation

Up to this point we have spent extensive effort assessing the skill of the MITgcm to reproduce the key forcing parameters listed in our introduction. This effort is motivated by the potential for using the MITgcm model output as a tool to improve our ability to model gas budgets in the IOBL and to improve our estimates of k in the sea ice zone, both of which depend on sea ice processes in the IOBL. To illustrate the potential impact that IOBL properties can have on the estimate of k, we perform a simple experiment, using estimates of k over the range of variation in model output at three locations in the sea ice zone. The intention is to illustrate the variability in k and in the radon deficit that can arise as a result of sea ice processes.

4.1 Constraining gas exchange forcings

Utilizing the results from section 3.1, 3.2 and 3.3, we calculated gas exchange velocities at P1, P2 and P3 (Figure 10), over the course of the model simulation (i.e. n = 2557 days * 3 = 7671) introduced in section 3.1. The MITgcm IOBL properties are fed to the estimator of k, considering sea ice processes (Loose et al. 2014). Our selected points have the mean sea ice concentrations of 96.1%, 87.62% and 61.69%, sea ice speeds of 0.05, 0.086 and 0.10 ms^{-1}, wind speeds of 8.73, 5.87 and 4.11 ms^{-1}.

The result yields a point cloud of values that vary depending primarily on the range of ice velocity, wind speed and sea ice cover. The values of k range between 0.1 and 14.0, a mean of 2.4 and standard deviation of 1.55. This exercise demonstrates the

sensitivity of k to the IOBL forcing parameters. In the event that we can trust the majority of the model outputs, such as the case here with high fidelity in the simulated SI concentration and SI velocities in A1, we conclude that, a numerical model, even a coarse resolution one, can make significant improvement to the estimate of k. The question of constraining the radon budget within a Lagrangian water parcel is somewhat more complicated.

4.2 Application of forcings on Radon budget

The results in Section 3.4 showed that the difference between model and data water trajectories accumulated too much error to be useful, and indicate that for a regional GCM to be useful for reconstructing the back trajectories of radon-labeled water parcels, we will need improved wind-forcing fields. With current reanalysis products, finding the back trajectory of radon-labeled water parcel is not feasible. When improved wind fields are available, the Green's functions approach (Menemenlis et al. 2005; Nguyen et al. 2011) or adjoint method (Forget et al. 2015, p. 4; Wunsch and Heimbach 2013) can be used to reduce misfits between modeled and observed MLD velocity and likely make the model a valuable tool for tracking back trajectories, either in a smaller domain or full Arctic regional configuration. A possible source of wind data can be from shipboard measurements, assuming the measurements persist over 10 days in the given sampling station.

However, it may be possible to improve on the existing approach. When the drift trajectory is not known, one solution is to resort to averaging IOBL properties within a radius that is equal to the 30-day drift track (e.g. as done by Rutgers Van Der Loeff et

al. 2014). The averages within this circle are treated as the representative IOBL properties. The radius of spatial averaging should be restricted by the average magnitude of the water parcel's velocity multiplied by the time span of interest. When applying a spatial averaging, if the time scale of changes in forcings is smaller than time span of interest, the time dependency of forcings should be accounted for. Typically sea ice velocity is ~ 5 times greater than vertically averaged water velocity in mixed layer (Cole et al. 2014). In this regard, it may be acceptable to assume that the water parcel is stationary as long as ice advection is accounted for. Hence spatial averaging, should account for ice drift over the point of radon/radium sampling. The same logic also applies to the changes in the MLD and sea ice concentration. For example, gas exchange calculated (Eq. 1) based on assumption of constant MLD of 27.5 m with limits of 5 to 50 m (Peralta-Ferriz and Woodgate 2015), would have limits of ±80%, whereas gas exchange calculated based on model MLD would have ±50% error and accounts for time variability. With the current level of uncertainty in reanalysis products and inherent heterogeneity of marginal sea ice zones, we suggest a mixed weighted combination of model outputs and shipboard data to be the way forward for constraining gas budget in sea ice zones.

5. Summary

We have used 36-km, 9km and 2km versions of the ECCO ocean-sea ice coupled models based on the MITgcm to investigate whether numerical model outputs can be used to compensate for lack of data in constraining air-sea gas exchange rate in the Arctic. The goal is to understand if model outputs can improve estimation of gas exchange velocity calculation and to evaluate the capability of the model to fill in the

missing information in radon deficiency method. This systematic comparison of upper ocean processes has revealed the following.

The coarse resolution model showed a good fidelity in regard to reproducing sea ice concentration. Depending on the location/season, the error of simulated ice concentration varied between 0.02 and 0.2. Away from ice fronts or active melting/freezing zones the model tended to have higher accuracy. Even in the marginal ice zone, due to the potentially high error in the satellite derived ice concentration, the model can still be used to quantify the air-sea gas exchange rate, though with an expected higher uncertainty due to the combination of model and data errors. In addition to sea ice concentration, we also found good correlation (82%) between model ice speed and ITP drift.

The estimation of mixed layer depth is challenging due to its dependence on unconstrained density anomaly or density gradient thresholds. No MLD algorithm performs well in all situations. In addition, CTD profiles from drifting buoys often do not include the top 7-10 m of the surface ocean where stratification can be important. Adding to the challenge is the dependence of the ocean density structure on vertical fluxes. In these model-data comparisons we found model MLD to be consistently biased on the shallower side in all model resolutions. We note however this result can partly be due to the missing upper 7m in moored drifters such as ITPs and thus resulting in a 1-sided bias in the observed MLD. The evolution of the mixing events showed that MLD correlates to sea ice fraction: in areas of nearly full ice cover, small openings may result in exposure of water to the cold atmosphere and the resulting freezing events would deepen the mixed layer via brine rejection. The higher the

resolution, the higher the capability of the model to capture these openings and the resulting deepening effects. The usage of the salt plume parameterization does not play an important role in determining the MLD.

The A1, A2 and A3 experiments consistently could not capture the water velocity observed in ITPs or Mooring. We speculate this discrepancy may be the result of the quality of the reanalysis wind products that are forcing these models. The wind products have been shown to have poor correlation with observed data at high frequencies. Considering that the response of near surface water is almost instantaneous to the wind forcing, low correlation in wind velocity would have direct impact on the modeled near surface water velocities and likely yield low correlations between modeled and observed ocean currents. On the other hand, the same wind fields at lower frequencies and on broader spatial scale have higher accuracy, as evidenced by the high correlation between the modeled and observed sea ice velocity.

Taking into accounts all the misfits through detailed model-data comparisons, we were able to quantify the usefulness of a numerical model to improve gas exchange rate and parameterization methods. We showed an example of how the sea ice concentration, velocity and mixed-layer depth can affect gas-exchange rate by up to 200% in marginal sea ice zones and that the model outputs can help constrain this rate. By finding the low correlation in near surface ocean velocities, irrespective of model horizontal resolution, we concluded that finding the back trajectory of radon labeled water parcels is currently not feasible. Furthermore, we speculate the source for the common errors in our models, namely the high frequency and under-constrained atmospheric forcing fields, as well as identify alternative approaches to enable the use

of a model to achieve the back trajectory calculation task. The alternative approach includes using the MITgcm Green's functions and adjoint capability to help constrain the model ocean velocity to observations, and performing the simulations in a smaller dedicated domain based on the specific spatial distribution of data for both atmospheric winds and ocean currents in the mixed layer.

References

Acreman, D. M., and C. D. Jeffery. 2007. "The Use of Argo for Validation and Tuning of Mixed Layer Models." *Ocean Modelling* 19 (1–2): 53–69. doi:10.1016/j.ocemod.2007.06.005.

Adcroft, Alistair, and Jean-Michel Campin. 2004. "Rescaled Height Coordinates for Accurate Representation of Free-Surface Flows in Ocean Circulation Models." *Ocean Modelling* 7 (3–4): 269–84. doi:10.1016/j.ocemod.2003.09.003.

Antonov, J, R Locarnini, T Boyer, A Mishonov, and H Garcia. n.d. "World Ocean Atlas 2005 Vol. 2 Salinity." *NOAA Atlas NESDIS* 62 (NOAA, Silver Spring, Md.).

Bender, Michael L., Saul Kinter, Nicolas Cassar, and Rik Wanninkhof. 2011. "Evaluating Gas Transfer Velocity Parameterizations Using Upper Ocean Radon Distributions." *Journal of Geophysical Research* 116 (C2). doi:10.1029/2009JC005805.

Blomquist, B. W., B. J. Huebert, C. W. Fairall, and I. C. Faloona. 2010. "Determining the Sea-Air Flux of Dimethylsulfide by Eddy Correlation Using Mass Spectrometry." *Atmospheric Measurement Techniques* 3: 1–20.

Boyer Montégut, Clément de, Gurvan Madec, Albert S. Fischer, Alban Lazar, and Daniele Iudicone. 2004. "Mixed Layer Depth over the Global Ocean: An Examination of Profile Data and a Profile-Based Climatology." *Journal of Geophysical Research: Oceans* 109 (C12): C12003. doi:10.1029/2004JC002378.

Brainerd, Keith E., and Michael C. Gregg. 1995. "Surface Mixed and Mixing Layer Depths." *Deep Sea Research Part I: Oceanographic Research Papers* 42 (9): 1521–43. doi:10.1016/0967-0637(95)00068-H.

Chaudhuri, Ayan H., Rui M. Ponte, and An T. Nguyen. 2014. "A Comparison of Atmospheric Reanalysis Products for the Arctic Ocean and Implications for Uncertainties in Air–Sea Fluxes." *Journal of Climate* 27 (14): 5411–21. doi:10.1175/JCLI-D-13-00424.1.

Cole, Sylvia T., Mary-Louise Timmermans, John M. Toole, Richard A. Krishfield, and Fredrik T. Thwaites. 2014. "Ekman Veering, Internal Waves, and Turbulence Observed under Arctic Sea Ice." *Journal of Physical Oceanography* 44 (5): 1306–28. doi:10.1175/JPO-D-12-0191.1.

Comiso, J. 2000. "Bootstrap Sea Ice Concentrations from Nimbus-7 SMMR and DMSP SSM/I-SSMIS." Boulder, Colorado USA: NASA DAAC at the National Snow and Ice Data Center.

Crabeck, Odile, B. Delille, S. Rysgaard, D. N. Thomas, N.-X. Geilfus, B. Else, and J.-L. Tison. 2014. "First 'in Situ' Determination of Gas Transport Coefficients (DO2, DAr, and DN2) from Bulk Gas Concentration Measurements (O2, N2, Ar) in Natural Sea Ice." *Journal of Geophysical Research: Oceans* 119 (10): 6655–68. doi:10.1002/2014JC009849.

Dong, Shenfu, Janet Sprintall, Sarah T. Gille, and Lynne Talley. 2008. "Southern Ocean Mixed-Layer Depth from Argo Float Profiles." *Journal of Geophysical Research: Oceans* 113 (C6): C06013. doi:10.1029/2006JC004051.

Fenty, Ian, and Patrick Heimbach. 2012. "Coupled Sea Ice–Ocean-State Estimation in the Labrador Sea and Baffin Bay." *Journal of Physical Oceanography* 43 (5): 884–904. doi:10.1175/JPO-D-12-065.1.

Forget, G., J.-M. Campin, P. Heimbach, C. N. Hill, R. M. Ponte, and C. Wunsch. 2015. "ECCO Version 4: An Integrated Framework for Non-Linear Inverse Modeling and Global Ocean State Estimation." *Geoscientific Model Development* 8 (10): 3071–3104. doi:10.5194/gmd-8-3071-2015.

Gerdes, Rüdiger, and Cornelia KöBerle. 2007. "Comparison of Arctic Sea Ice Thickness Variability in IPCC Climate of the 20th Century Experiments and in Ocean-Sea Ice Hindcasts." *Journal of Geophysical Research (Oceans)* 112 (April): C04S13. doi:10.1029/2006JC003616.

Heimbach, Patick, Dimitris Menemenlis, Martin Losch, Jean-Michel Campin, and Chris Hill. 2010. "On the Formulation of Sea-Ice Models. Part 2: Lessons from Multi-Year Adjoint Sea-Ice Export Sensitivities through the Canadian Arctic Archipelago." *Ocean Modelling* 33 (1-2): 145–58. doi:10.1016/j.ocemod.2010.02.002.

H. J. Zemmelink, B. Delille, J. L. Tison, E. J. Hintsa, L. Houghton, and J. W.H. Dacey. 2006a. "CO_2 Deposition over Multi-Year Ice of the Western Weddell Sea." *Geophysical Research Letters* 33. doi:10.1029/2006GL026320.

———. 2006b. "CO_2 Deposition over Multi-Year Ice of the Western Weddell Sea." *Geophysical Research Letters* 33. doi:10.1029/2006GL026320.

Ho, D. T., C. S. Law, M. J. Smitth, P. Schlosser, M. Harvey, and P. Hill. 2006. "Measurements of Air-Sea Gas Exchange at High Wind Speeds in the Southern Ocean: Implications for Global Parameterizations." *Geophysical Research Letters* 33. doi:10.1029/2006GL026817.

Hyndman, Rob J., and Anne B. Koehler. 2006. "Another Look at Measures of Forecast Accuracy." *International Journal of Forecasting* 22 (4): 679–88. doi:10.1016/j.ijforecast.2006.03.001.

Ivanova, N., L. T. Pedersen, R. T. Tonboe, S. Kern, G. Heygster, T. Lavergne, A. Sørensen, et al. 2015. "Inter-Comparison and Evaluation of Sea Ice Algorithms: Towards Further Identification of Challenges and Optimal Approach Using Passive Microwave Observations." *The Cryosphere* 9 (5): 1797–1817. doi:10.5194/tc-9-1797-2015.

Jackson, J. M., E. C. Carmack, F. A. McLaughlin, S. E. Allen, and R. G. Ingram. 2010. "Identification, Characterization, and Change of the near-Surface Temperature Maximum in the Canada Basin, 1993–2008." *Journal of Geophysical Research* 115 (C5). doi:10.1029/2009JC005265.

Jähne, B., and H. Haubecker. 1998. "Air-Water Gas Exchange." *Annual Review of Fluid Mechanics* 30: 443–48. doi:10.1146/annurev.fluid.30.1.443.

Johnson, Mark, Steve Gaffigan, Elizabeth Hunke, and Ruediger Gerdes. 2007. "A Comparison of Arctic Ocean Sea Ice Concentration among the Coordinated AOMIP Model Experiments." *Journal of Geophysical Research: Oceans* 112 (C4): C04S11. doi:10.1029/2006JC003690.

Johnson, Mark, Andrey Proshutinsky, Yevgeny Aksenov, An T. Nguyen, Ron Lindsay, Christian Haas, Jinlun Zhang, et al. 2012. "Evaluation of Arctic Sea Ice Thickness Simulated by Arctic Ocean Model Intercomparison Project Models." *Journal of Geophysical Research* 117 (March). doi:10.1029/2011JC007257.

Kara, A. Birol. 2003. “Mixed Layer Depth Variability over the Global Ocean.” *Journal of Geophysical Research* 108 (C3). doi:10.1029/2000JC000736.

Kohout, A. L., and M. H. Meylan. 2008. “An Elastic Plate Model for Wave Attenuation and Ice Floe Breaking in the Marginal Ice Zone.” *Journal of Geophysical Research* 113. doi:10.1029/2007JC004434.

Krishfield, R. A., A. Proshutinsky, K. Tateyama, W. J. Williams, E. C. Carmack, F. A. McLaughlin, and M.-L. Timmermans. 2014. “Deterioration of Perennial Sea Ice in the Beaufort Gyre from 2003 to 2012 and Its Impact on the Oceanic Freshwater Cycle.” *Journal of Geophysical Research: Oceans* 119 (2): 1271–1305. doi:10.1002/2013JC008999.

Krishfield, R., J. Toole, A. Proshutinsky, and M-L. Timmermans. 2008. “Automated Ice-Tethered Profilers for Seawater Observations under Pack Ice in All Seasons.” *Journal of Atmospheric and Oceanic Technology* 25 (11): 2091–2105. doi:10.1175/2008JTECHO587.1.

Large, W. G., J. C. McWilliams, and S. C. Doney. 1994. “Oceanic Vertical Mixing: A Review and a Model with a Nonlocal Boundary Layer Parameterization.” *Reviews of Geophysics* 32 (4): 363–403. doi:10.1029/94RG01872.

Legge, Oliver J., Dorothee C. E. Bakker, Martin T. Johnson, Michael P. Meredith, Hugh J. Venables, Peter J. Brown, and Gareth A. Lee. 2015. “The Seasonal Cycle of Ocean-Atmosphere CO2 Flux in Ryder Bay, West Antarctic Peninsula.” *Geophysical Research Letters* 42 (8): 2015GL063796. doi:10.1002/2015GL063796.

Lindsay, Ron, Mark Wensnahan, A. Schweiger, and J. Zhang. 2014. “Evaluation of Seven Different Atmospheric Reanalysis Products in the Arctic*.” *Journal of Climate* 27 (7): 2588–2606.

Lindsay, R. W., and D. A. Rothrock. 1995. “Arctic Sea Ice Leads from Advanced Very High Resolution Radiometer Images.” *Journal of Geophysical Research* 100: 4533–44.

Locarnini, R, J Mishonov, T Boyer, J.I. Antonov, and H. E. Garcia. n.d. “World Ocean Atlas 2005 Vol. 1 Temreature.” *NOAA Atlas NESDIS* 62 (NOAA, Silver Spring, Md.).

Loose, B, R Kelly, A Bigdeli, R.A Krishfield, M Rutgers Van Der Loeff, and B Moran. 2016. "How Well Does Wind Speed Predict Air-Sea Gas Transfer in the Sea Ice Zone? A Synthesis of Radon Deficit Profiles in the Upper Water Column of the Arctic Ocean," no. Accepted.

Loose, B., W. R. McGillis, D. Perovich, C. J. Zappa, and P. Schlosser. 2014. "A Parameter Model of Gas Exchange for the Seasonal Sea Ice Zone." *Ocean Science* 10 (1): 1–16. doi:10.5194/os-10-1-2014.

Loose, B., W. R. McGillis, P. Schlosser, D. Perovich, and T. Takahashi. 2009. "Effects of Freezing, Growth, and Ice Cover on Gas Transport Processes in Laboratory Seawater Experiments." *Geophysical Research Letters* 36 (5): L05603. doi:10.1029/2008GL036318.

Loose, B., P. Schlosser, D. Perovich, D. Ringelberg, D.t. Ho, T. Takahashi, J. Richter-Menge, C.m. Reynolds, W.r. Mcgillis, and J.-L. Tison. 2011. "Gas Diffusion through Columnar Laboratory Sea Ice: Implications for Mixed-Layer Ventilation of CO2 in the Seasonal Ice Zone." *Tellus B* 63 (1): 23–39. doi:10.1111/j.1600-0889.2010.00506.x.

Lorbacher, K., D. Dommenget, P. P. Niiler, and A. Köhl. 2006. "Ocean Mixed Layer Depth: A Subsurface Proxy of Ocean-Atmosphere Variability." *Journal of Geophysical Research: Oceans* 111 (C7): C07010. doi:10.1029/2003JC002157.

Losch, Martin, Dimitris Menemenlis, Jean-Michel Campin, Patick Heimbach, and Chris Hill. 2010. "On the Formulation of Sea-Ice Models. Part 1: Effects of Different Solver Implementations and Parameterizations." *Ocean Modelling* 33 (1-2): 129–44. doi:10.1016/j.ocemod.2009.12.008.

Marshall, John, Alistair Adcroft, Chris Hill, Lev Perelman, and Curt Heisey. 1997. "A Finite-Volume, Incompressible Navier Stokes Model for Studies of the Ocean on Parallel Computers." *Journal of Geophysical Research: Oceans* 102 (C3): 5753–66. doi:10.1029/96JC02775.

McPhee, M. G., A. Proshutinsky, J. H. Morison, M. Steele, and M. B. Alkire. 2009. "Rapid Change in Freshwater Content of the Arctic Ocean." *Geophysical Research Letters* 36: L04606. doi:10.1029/2008GL036587.

McPhee, Miles G. 2012. “Advances in Understanding Ice–ocean Stress during and since AIDJEX.” *Cold Regions Science and Technology* 76-77 (June): 24–36. doi:10.1016/j.coldregions.2011.05.001.

McPhee, M., and D. G. Martinson. 1992. “Turbulent Mixing under Drifting Pack Ice in the Weddell Sea.” *Science* 263: 218–20.

Menemenlis, Dimitris, J.-M. Campin, Patrick Heimbach, Chris Hill, Tong Lee, An Nguyen, Michael Schodlok, and Hong Zhang. 2008. “ECCO2: High Resolution Global Ocean and Sea Ice Data Synthesis.” *Mercator Ocean Quarterly Newsletter* 31: 13–21.

Menemenlis, Dimitris, Ichiro Fukumori, and Tong Lee. 2005. “Using Green’s Functions to Calibrate an Ocean General Circulation Model.” *Monthly Weather Review* 133 (5): 1224–40. doi:10.1175/MWR2912.1.

Nguyen, An T., Ronald Kwok, and Dimitris Menemenlis. 2012. “Source and Pathway of the Western Arctic Upper Halocline in a Data-Constrained Coupled Ocean and Sea Ice Model.” *Journal of Physical Oceanography* 42 (5): 802–23. doi:10.1175/JPO-D-11-040.1.

Nguyen, An T., Dimitris Menemenlis, and Ronald Kwok. 2011. “Arctic Ice-Ocean Simulation with Optimized Model Parameters: Approach and Assessment.” *Journal of Geophysical Research: Oceans* 116 (C4): C04025. doi:10.1029/2010JC006573.

Nguyen, A. T., D. Menemenlis, and R. Kwok. 2009. “Improved Modeling of the Arctic Halocline with a Subgrid-Scale Brine Rejection Parameterization.” *Journal of Geophysical Research* 114 (C11). doi:10.1029/2008JC005121.

Nightingale, Philip D., G. M. Malin, Cliff Law, Andrew Watson, P. S. Liss, M. I. Liddicoat, J. Boutin, and Robert C. Upstill-Goddard. 2000a. “In Situ Evaluation of Air-Sea Gas Exchange Parameterizations Using Novel Conservative and Volatile Tracers.” *Global Biogeochemical Cycles* 14: 373–87.

———. 2000b. “In Situ Evaluation of Air-Sea Gas Exchange Parameterizations Using Novel Conservative and Volatile Tracers.” *Global Biogeochemical Cycles* 14: 373–87.

Ohno, Yuko, Naoto Iwasaka, Fumiaki Kobashi, and Yoshiko Sato. 2008. "Mixed Layer Depth Climatology of the North Pacific Based on Argo Observations." *Journal of Oceanography* 65 (1): 1–16. doi:10.1007/s10872-009-0001-4.

Onogi, Kazutoshi, Junichi Tsutsui, Hiroshi Koide, Masami Sakamoto, Shinya Kobayashi, Hiroaki Hatsushika, Takanori Matsumoto, et al. 2007. "The JRA-25 Reanalysis." *Journal of the Meteorological Society of Japan. Ser. II* 85 (3): 369–432. doi:10.2151/jmsj.85.369.

Peng, Ts-H., W. S. Broecker, G. G. Mathieu, and Y.-H. Li. 1979. "Radon Evasion Rates in the Atlantic and Pacific Oceans as Determined during the Geosecs Program." *Journal of Geophysical Research* 84: 2471–86.

Peralta-Ferriz, Cecilia, and Rebecca A. Woodgate. 2015. "Seasonal and Interannual Variability of Pan-Arctic Surface Mixed Layer Properties from 1979 to 2012 from Hydrographic Data, and the Dominance of Stratification for Multiyear Mixed Layer Depth Shoaling." *Progress in Oceanography* 134 (May): 19–53. doi:10.1016/j.pocean.2014.12.005.

Perovich, D., G. A. Maykut, 1990. "Solar Heating of a Stratified Ocean in the Presence of a Static Ice Cover." *Journal of Geophysical Research* 95 (C10): 18233–45. doi:10.1029/JC095iC10p18233.

Proshutinsky, A., Rüdiger Gerdes, D. Holland, G. Holloway, and M. Steele. 2008. "AOMIP: Coordinated Activities to Improve Models and Model Predictions." *CLIVAR Exchanges, 13(1). (Exchanges ; 44)* 17. http://eprints.soton.ac.uk/50120/01/Exch_44.pdf.

Proshutinsky, Andrey, Richard Krishfield, Mary-Louise Timmermans, John Toole, Eddy Carmack, Fiona McLaughlin, William J. Williams, Sarah Zimmermann, Motoyo Itoh, and Koji Shimada. 2009. "Beaufort Gyre Freshwater Reservoir: State and Variability from Observations." *Journal of Geophysical Research* 114 (June). doi:10.1029/2008JC005104.

Proshutinsky, Andrey, Michael Steele, Jinlun Zhang, Gregory Holloway, Nadja Steiner, Sirpa Hakkinen, David Holland, et al. 2001. "Multinational Effort Studies Differences among Arctic

Ocean Models." *Eos, Transactions American Geophysical Union* 82 (51): 637–44. doi:10.1029/01EO00365.

Rutgers Van Der Loeff, Michiel, Nicolas Cassar, Marcel Nicolaus, Benjamin Rabe, and I. Stimac. 2014. "The Influence of Sea Ice Cover on Air-Sea Gas Exchange Estimated with Radon-222 Profiles." *Journal of Geophysical Research - Oceans* 119: 2735–51. doi:10.1002/2013JC009321.

Salter, M. E., R. C. Upstill-Goddard, P. D. Nightingale, S. D. Archer, B. Blomquist, D. T. Ho, B. Huebert, P. Schlosser, and M. Yang. 2011. "Impact of an Artificial Surfactant Release on Air-Sea Gas Fluxes during Deep Ocean Gas Exchange Experiment II." *Journal of Geophysical Research* 116: C11016. doi:10.1029/2011JC007023.

Shaw, W. J., T. P. Stanton, M. G. McPhee, J. H. Morison, and D. G. Martinson. 2009. "Role of the Upper Ocean in the Energy Budget of Arctic Sea Ice during SHEBA." *Journal of Geophysical Research* 114 (C6). doi:10.1029/2008JC004991.

Shimada, Koji, Eddy C. Carmack, Kiyoshi Hatakeyama, and Takatoshi Takizawa. 2001. "Varieties of Shallow Temperature Maximum Waters in the Western Canadian Basin of the Arctic Ocean." *Geophysical Research Letters* 28 (18): 3441–44.

Smethie, William M., Taro Takahashi, David W. Chipman, and James R. Ledwell. 1985. "Gas Exchange and CO2 Flux in the Tropical Atlantic Ocean Determined from 222Rn and pCO2 Measurements." *Journal of Geophysical Research: Oceans (1978–2012)* 90 (C4): 7005–22.

Spall, Michael A., Robert S. Pickart, Paula S. Fratantoni, and Albert J. Plueddemann. 2008. "Western Arctic Shelfbreak Eddies: Formation and Transport." *Journal of Physical Oceanography* 38 (8): 1644–68. doi:10.1175/2007JPO3829.1.

Sweeney, C., E. Gloor, A. R. Jacobson, R. M. Key, G. McKinley, J.-L. Sarmiento, and R. Wanninkhof. 2007. "Constraining Global Air-Sea Gas Exchange for CO2 with Recent Bomb 14C Measurements." *Global Biogeochemical Cycles* 21. doi:10.1029/2006GB002784.

Takahashi, Taro, Stewart C. Sutherland, Rik Wanninkhof, Colm Sweeney, Richard A. Feely, David W. Chipman, Burke Hales, et al. 2009. “Climatological Mean and Decadal Change in Surface Ocean pCO_2, and Net Sea-Air CO_2 Flux over the Global Oceans.” *Deep-Sea Research Part II* 56: 554–77.

Thomson, Richard E., and Isaac V. Fine. 2003. “Estimating Mixed Layer Depth from Oceanic Profile Data.” *Journal of Atmospheric and Oceanic Technology* 20 (2): 319–29. doi:10.1175/1520-0426(2003)020<0319:EMLDFO>2.0.CO;2.

Timmermans, M.-L., A. Proshutinsky, R. A. Krishfield, D. K. Perovich, J. A. Richter-Menge, T. P. Stanton, and J. M. Toole. 2011. “Surface Freshening in the Arctic Ocean’s Eurasian Basin: An Apparent Consequence of Recent Change in the Wind-Driven Circulation.” *Journal of Geophysical Research* 116 (July). doi:10.1029/2011JC006975.

Toole, J. M., M. L. Timmermans, D. K. Perovich, R. A. Krishfield, A. Proshutinsky, and J. A. Richter-Menge. 2010. “Nfluences of the Ocean Surface Mixed Layer and Thermohaline Stratification on Arctic Sea Ice in the Central Canada Basin.” *Journal of Geophysical Research* 115. doi:10.1029/2009JC005660.

Wadhams, P., V. A. Squire, J. A. Ewing, and R. W. Pascal. 1986. “The Effect of the Marginal Ice Zone on the Directional Wave Spectrum of the Ocean.” *Journal of Physical Oceanography* 16: 358–76.

Wanninkhof, Rik. 1992. “Relationship between Wind Speed and Gas Exchange over the Ocean.” *Journal of Geophysical Research: Oceans* 97 (C5): 7373–82. doi:10.1029/92JC00188.

Wanninkhof, R., and W. R. McGillis. 1999. “A Cubic Relationship between Air-Sea CO2 Exchangeand Wind Speed.” *Geophysical Research Letters* 26: 1889–92.

Wijesekera, Hemantha W., and Michael C. Gregg. 1996. “Surface Layer Response to Weak Winds, Westerly Bursts, and Rain Squalls in the Western Pacific Warm Pool.” *Journal of Geophysical Research: Oceans* 101 (C1): 977–97. doi:10.1029/95JC02553.

Williams, A. J., F. T. Thwaites, A. T. Morrison, J. M. Toole, and R. A. Krishfield. 2010. “Motion Tracking in an Acoustic Point-Measurement Current Meter.” In . IEEE. doi:10.1109/OCEANSSYD.2010.5603862.

Wunsch, Carl, and Patrick Heimbach. 2013. “Dynamically and Kinematically Consistent Global Ocean Circulation and Ice State Estimates.” In *In Ocean Circulation and Climate: A 21 Century Perspective*. Elsevier BV. https://dash.harvard.edu/handle/1/12136112.

Zemmelink, H. J., J. W. H. Dacey, L. Houghton, E. J. Hintsa, and P. S. Liss. 2008. “Dimethylsulfide Emissions over the Multi-Year Ice of the Western Weddell Sea.” *Geophysical Research Letters* 35. doi:10.1029/2007GL031847.

Zhang, Jinlun, and D. A. Rothrock. 2003. “Modeling Global Sea Ice with a Thickness and Enthalpy Distribution Model in Generalized Curvilinear Coordinates.” *Monthly Weather Review* 131 (5): 845–61. doi:10.1175/1520-0493(2003)131<0845:MGSIWA>2.0.CO;2.

Zhao, Mengnan, and Mary-Louise Timmermans. 2015. “Vertical Scales and Dynamics of Eddies in the Arctic Ocean’s Canada Basin.” *Journal of Geophysical Research: Oceans* 120 (12): 8195–8209. doi:10.1002/2015JC011251.

Zhao, Mengnan, Mary-Louise Timmermans, Sylvia Cole, Richard Krishfield, Andrey Proshutinsky, and John Toole. 2014. “Characterizing the Eddy Field in the Arctic Ocean Halocline.” *Journal of Geophysical Research: Oceans* 119 (12): 8800–8817. doi:10.1002/2014JC010488.

Zhao, Mengnan, Mary-Louise Timmermans, Sylvia Cole, Richard Krishfield, and John Toole. 2016. “Evolution of the Eddy Field in the Arctic Ocean’s Canada Basin, 2005–2015.” *Geophysical Research Letters* 43 (15): 2016GL069671. doi:10.1002/2016GL069671.

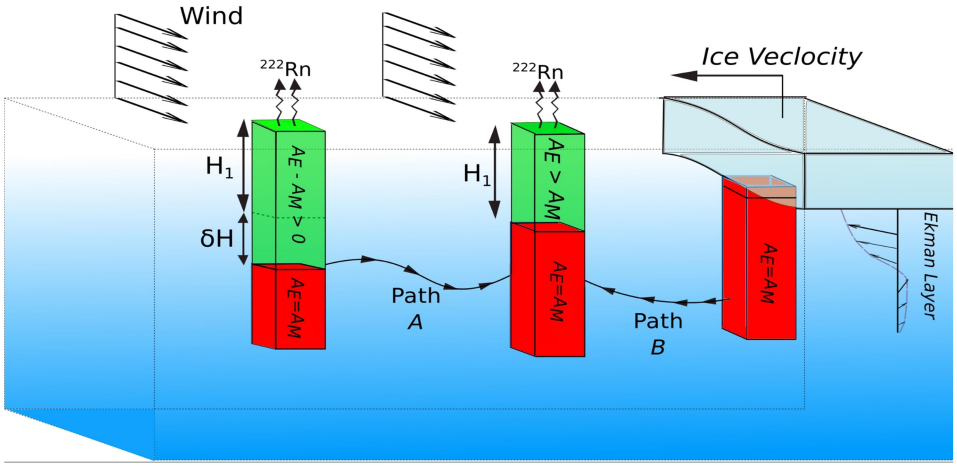

Figure 1 A graphic illustration of two possible back trajectory for a single sampling

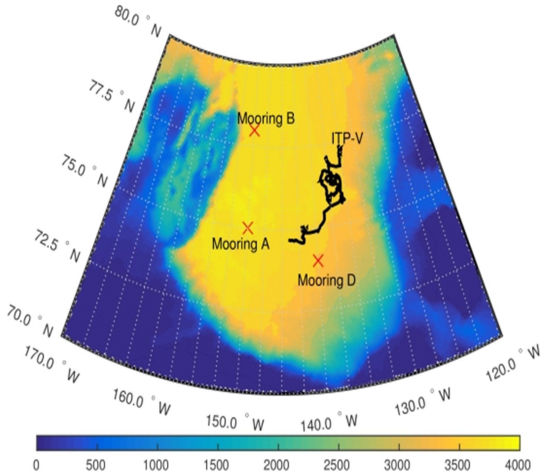

Figure 2: Bathymetry and location of ITP-V and Mooring for data comparison

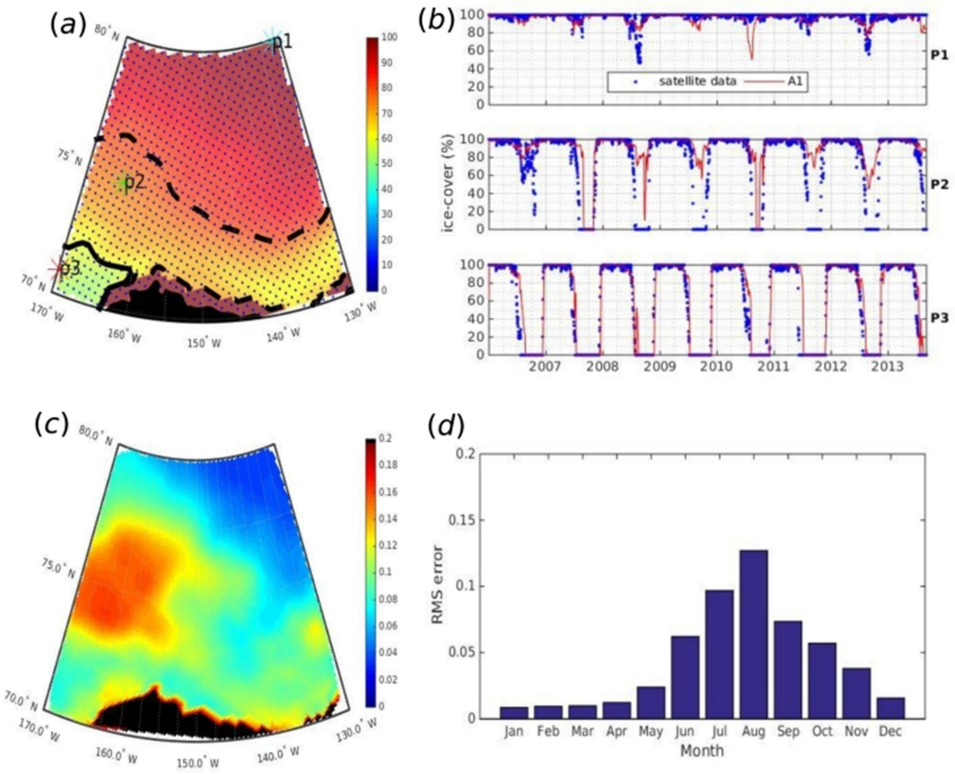

Figure 3 . (a) Averaged satellite sea ice cover from 2006-2013, Solid black line marking 60% cover and dashed black line marking 80%, Blue dots show the analysis grid, stars show the location of the three points Cyan P1, Green P2, Red P3 where time series data is graphed in b. (b)Time history of Sea-Ice fraction from top P1, P2 and P3, Satellite data represented by blue dots, compared with A1(c) Horizontal distribution of RMS error of A1 sea ice concentration averaged over time from 2006 to 2013; black mask covers the grid points on the land, (d) Spatially averaged Annual RMS error of A1 sea ice concentration.

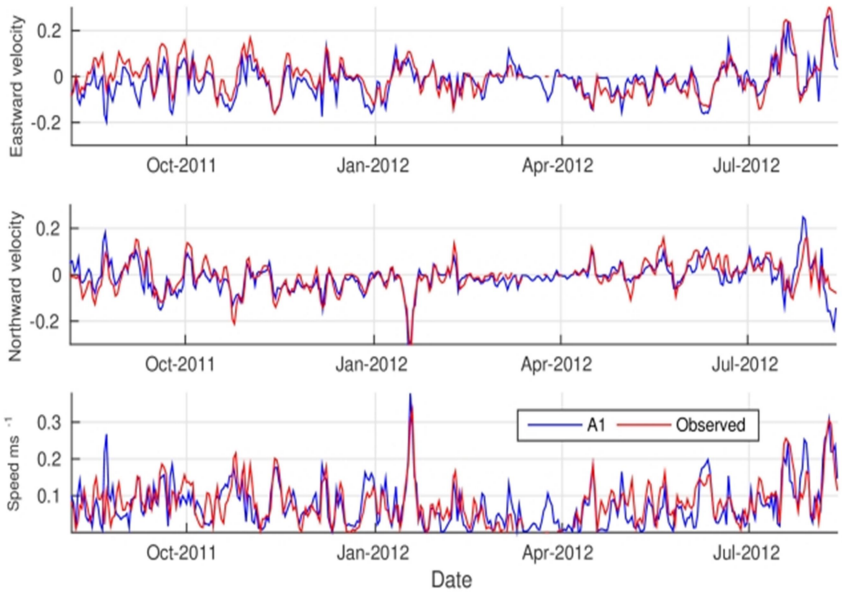

Figure 4: Time series of sea ice velocity components and speed of ITP 53 vs. 36 km horizontal resolution of MITgcm (A1). The correlations between eastward, northward and magnitude of velocity between ITP 53 data and A1 are 78%,75% and 80%, respectively.

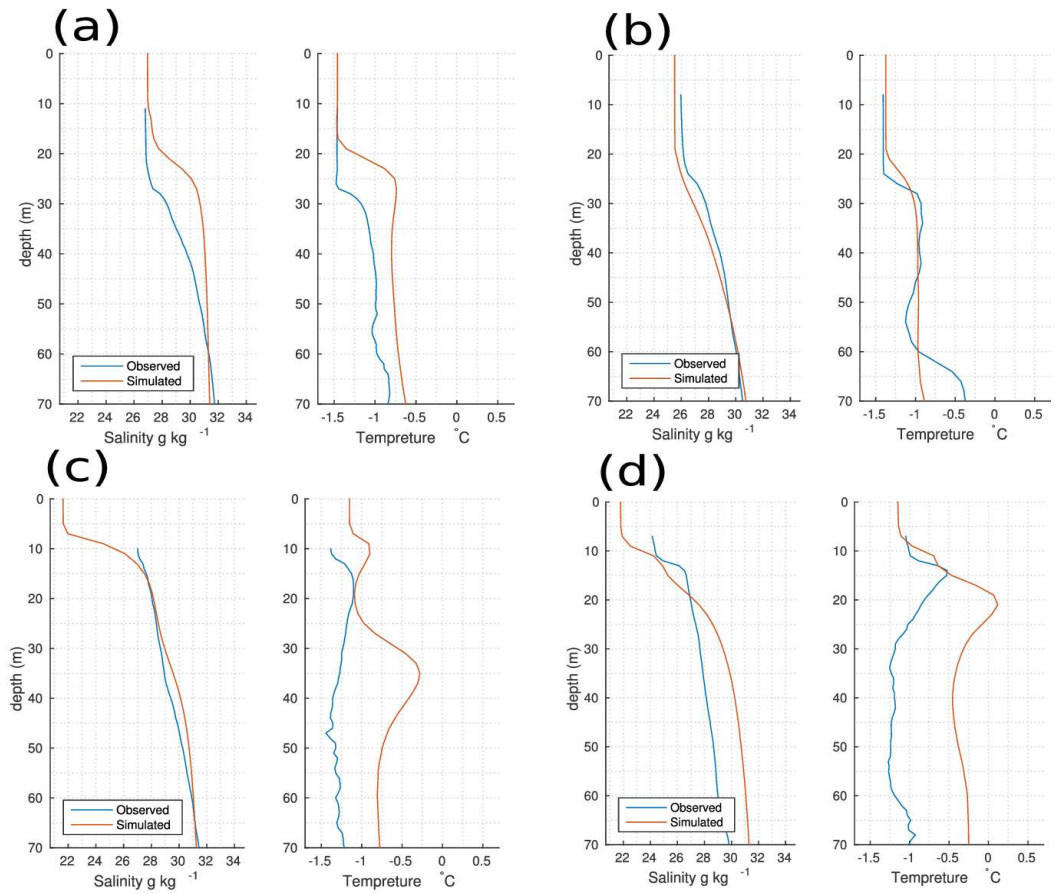

Figure 5 Salinity and Temperature of top 70 m based on ITPs and A1 (a) ITP 1 on 13-Dec-2006 at 74.80°N and 131.44°W (b) ITP-43 on 27-Nov-2010 at 75.41°N and 143.09°W (c)ITP 1 on 28-Aug-2006 at 76.96°N and 133.32°W (d) ITP-13 on 30-Jul-2008 at 75.00°N and 132.78°W

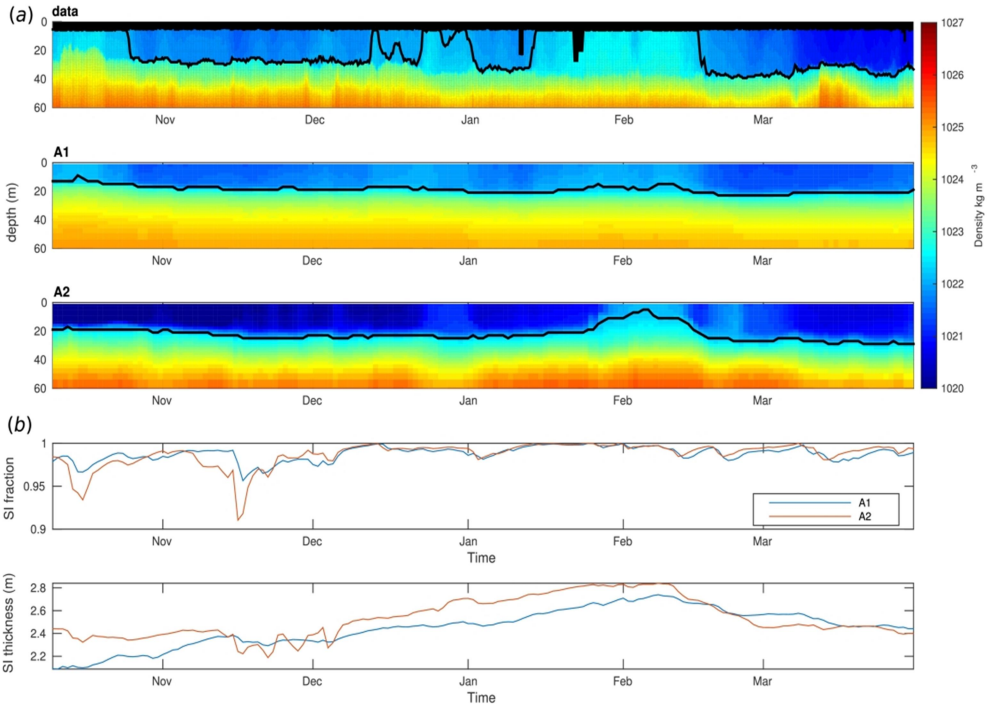

Figure 6 (a) Observed upper ocean density vs 36 km(A1) and 9 km(A2) resolution MITgcm density along the path of ITP drift, black mask covers areas that no ITP data is available and solid black line shows isopycnal of 1022.5 kgm-3 . (b) Simulated sea ice fraction and thickness on top of the water column

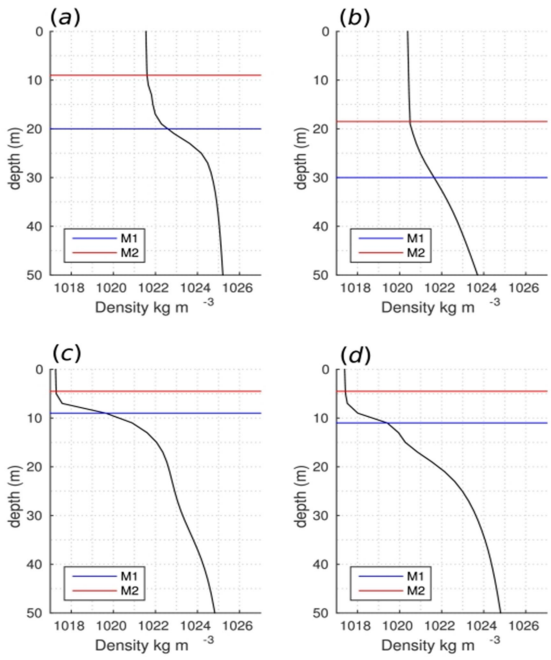

Figure 7 Methods M1 and M2 applied to selected ITP profiles,(a) ITP 1 on 13-Dec-2006 at 74.80°N and 131.44°W (b) ITP-43 on 27-Nov-2010 at 75.41°N and 143.09°W (c)ITP 1 on 28-Aug-2006 at 76.96°N and 133.32°W (d) ITP-13 on 30-Jul-2008 at 75.00°N and 132.78°W.

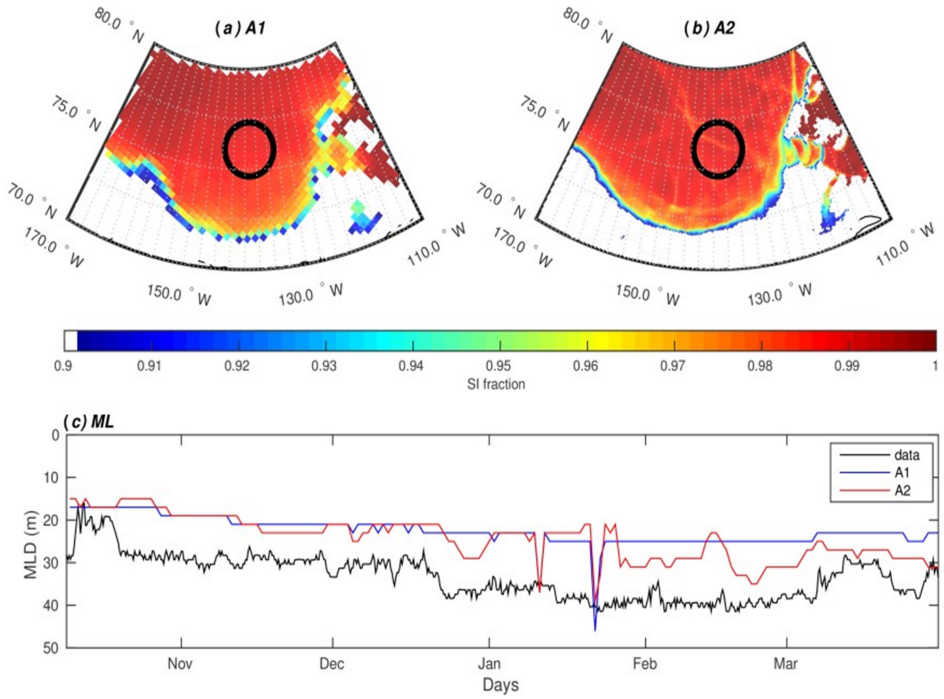

Figure 8 Sea ice cover higher than 0.9 with gray circle marking the area of ITP operation for (a) 36 km (A1) and (b) 9 km(A2) horizontal resolution of the model. A2 captured the ice opening and resulting mixed layer change while this phenomena has been averaged out by coarse resolution model (c) observed and simulated evolution of mixed layer depth on the path of ITP

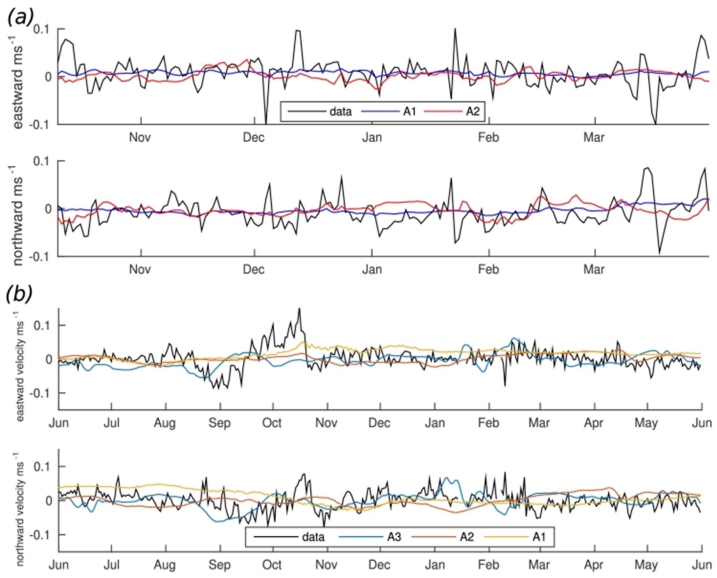

Figure 9 (a) Daily averaged velocity components from 5 to 50 meters observed by ITP-V vs simulated by A1 and A2 (b) Daily averaged velocity components at 25 meters observed by mooring D vs A1,A2 and A3.

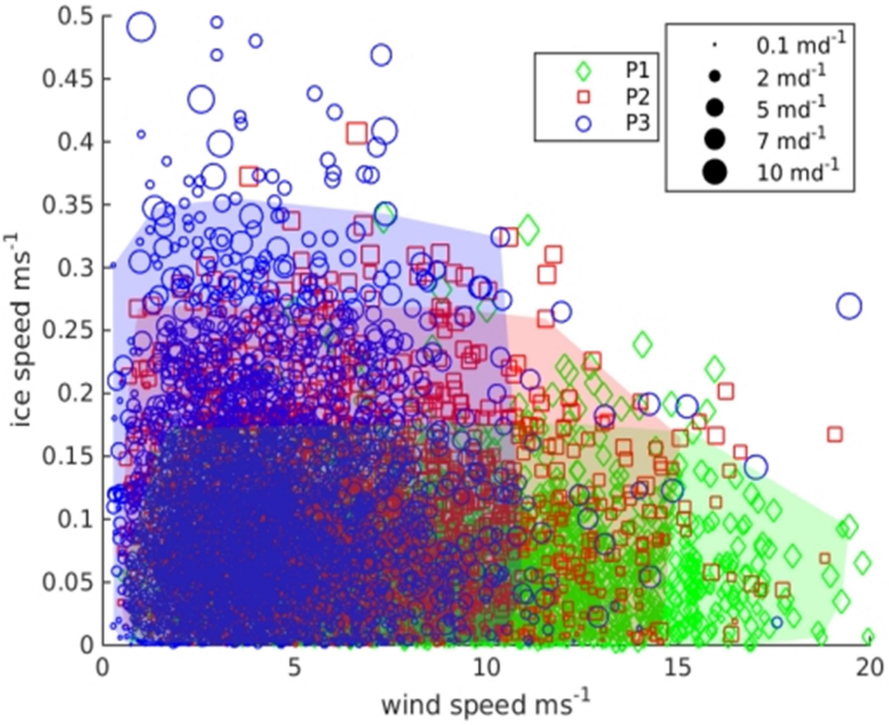

Figure 10 Gas exchange estimated model outputs of wind and sea ice speed at locations P1: 77.4N 143.6W, P2: 74.8N 163.5W and P3: 70.59N 159.4W from Jan-2006 to Dec-2012 , Areas enclose the outputs around the mean and two standard deviation. The size of the points demonstrate the magnitude of the gas exchange velocities normalized by sea ice

Manuscript II

Forward and inverse modeling of near surface gas budgets in marginal ice zones, from gas exchange to mixing

Prepared to submission to Global Biogeochemical Cycles

A. Bigdeli[1], B. Loose[1],An T Nguyen[2]

[1]Graduate School of Oceanography, University of Rhode Island, Rhode Island, 02882, U.S.A

[2]University of Texas at Austin, Austin, Texas, 78712, US

Abstract

The interpretation of upper ocean geochemical gas budgets in marginal ice zones are often challenging due to the impact from a combination of environmental forcings acting on these budgets. While gas exchange may be the lead forcing, changes in stratification, ice cover, and modifications of the gas budget during sea ice melt (freeze) also play a role. To investigate the impact of these other forcings, we utilized a 1D numerical model based on MIT General Circulation Model (MITgcm) code and its inverse model to simulate the sampling conditions of 53 vertical radon profiles. The comparison of simulated hydrography and available data using an unconstrained model showed sensitivity of the budgets to the initial hydrography. The optimization based on the inversion model reduced uncertainties in initial conditions and supported the 1D model. Based on model outputs, we quantified the error introduced by ignoring the effects of advection, melt, and changes in mixed layer depth. We showed, without the insight from the numerical model, the gas budgets in areas with more than 80% ice cover, may have errors up to 50%. We further showed, in comparison to the radon data, current formulation of gas exchange velocity, under predicts gas fluxes in almost fully covered areas. Our results suggest that the numerical model and its inversion are necessary tools in interpreting near surface budgets in sea ice zones; specifically in almost fully covered regions.

1 Introduction

Mixed layer (ML) budget of biogeochemical gases in high latitude region has revived attention recently due to the impact biogenic gases such as CO_2 (Bates et al., 2011; Bates & Mathis, 2009; Detoni et al., 2015; Geilfus et al., 2012), O_2 (Castro-Morales et al., 2013) and methane (Kitidis et al., 2010; Shakhova et al., 2010) have on global climate. In addition to their climatological impact, geochemical gas budgets offer a mean to understand fundamental processes occurring in the ML such as rate of ventilation (Loose et al., 2017; Rutgers Van Der Loeff et al., 2014) and surface-deep ocean exchange (Abelmann et al., 2015).

In the open ocean a series of assumptions including horizontal homogeneity and steady state conditions makes determination and interpretation of the biogeochemical budgets straight forward (Peng et al., 1979; Smethie et al., 1985). Even though gas exchange velocity, due its dependence on wind (Wanninkhof, 2014), can vary with high frequency compared to budget renewal time, it has been shown that by applying a weighted average on this forcing, a steady state condition can be assumed with <20% error (Bender et al., 2011). The weights in this method are based on ventilation ratio of a constant ML depth (Reuer et al., 2007). Hence, the steady state condition is a valid assumption where the ML depth can be assumed near constant. This assumption holds well on time scales shorter than a seasonal cycle where atmospheric forcing gradually changes the ML depth (Acreman & Jeffery, 2007; Kara, 2003; Ohno et al., 2008).

In sea ice zones, on the other hand, the ML depth changes on shorter time scale due to freezing/melting of sea ice (Cole et al., 2014; Peralta-Ferriz & Woodgate, 2015; Toole et al., 2010; Vivier et al., 2016). Brine/freshwater input into the ocean surface

deepens/shoals the ML in span of a few days. This transient condition contradicts the steady state assumption of constant ML depth. Previously, physical numerical ocean models demonstrated the ability to capture these short time scale changes in the ML. For example, Fer et al. (2017) have used forward numerical 1D models to study turbulent heat and momentum transfer in sea ice zones, though constraining the gas budgets was not part of their investigation.

A shortcoming in using a forward unconstrained 1D model to capture ML depth changes and its effect on gas budgets is the highly unconstrained ambient conditions, such as initial vertical profile of salinity (S) and temperature (T) (Dwivedi et al., 2011), that dictate the initial ML depth and initial gas inventory. An inversion framework, on the other hand, can be used to obtain a set of initial conditions that are consistent with relevant observation (Nguyen et al., 2017). Here we utilize a 1D model based on MIT General Circulation Model (MITgcm) code and its non-linear inversion (also known as adjoint) framework (Forget et al., 2015b; Nguyen et al., 2017; Wunsch & Heimbach, 2007, 2013) to estimate the initial T & S profiles and study the effects of environmental forcing, such as changes in ML depth and sea ice melt/freeze on gas budgets.

A suitable approach to investigate the individual contribution of environmental forcing on the gas budgets is to quantify the inventory of near surface radon. Radon is an inert gas, does not participate in biology, and the half-life of radon (3.82 days) allows us to limit the simulations of the physical ocean conditions to 40 days i.e. 5 half-lives of radon.

Sampling of radon budgets is part of a geochemical method called the “Radon deficit method” (Bender et al., 2011; Peng et al., 1979). This method has been used in the open ocean and sea ice zones to determine the gas transfer velocity (Loose et al., 2017; Rutgers Van Der Loeff et al., 2014). The exchange transfer velocity inferred from these profiles suggests that, in contrast to other independent measurements (Butterworth & Miller, 2016; Prytherch et al., 2017), in marginal ice zones, wind speed parametrization of gas exchange velocity does not hold. We can investigate if the previously mentioned environmental forcings have distorted the inferred gas transfer velocity. We also quantify the impact these environmental forcing conditions: wind, sea ice cover, sea ice freeze/melt, and changes in ML depth, can have on the upper ocean budget of dissolved gas. We use the 1D MITgcm to simulate gas budgets as a function of upper ocean processes, and we use the 1D adjoint to tune the 40-day history of the environmental forcing to match observations at the time of sampling

In section 2.1 we introduce the 1D physical ocean numerical model and its adjoint. In Section 2.2 we give a background on the radon deficit method and current 1D control volume estimates of gas budgets. In section 3.1 we show the adjoint optimization results. In section 3.2 we compare the forward model outputs with available data and discuss the accuracy of control volume estimates. Finally in section 4 we provide a summary and an outlook perspective of our work

2-Method

2-1 MODEL Description

For this study we use the estimation framework existing within the Estimation of Circulation and Climate of the Ocean (ECCO) consortium (Wunsch & Heimbach, 2007, 2013). The forward model is based on an evolved version of the MIT general circulation model (MITgcm) (Adcroft et al., 2004; Marshall et al., 1997). Sea ice is simulated using MITgcm's sea ice package (Patick Heimbach et al., 2010; Losch et al., 2010).

The 1-D column configuration employs z coordinate system (Adcroft & Campin, 2004) with 0.5 m evenly spaced vertical nodes spanning from the surface down to 200m depth. Vertical mixing uses the K Profile Parametrization (KPP) (Large et al., 1997). Atmospheric forcing comes from JRA55 (Kobayashi et al., 2015). Brine rejection during sea-ice formation follows an updated parameterization of Nguyen et al., (2009). Bigdeli et al. (2017) have shown that the 1-D column is able to reproduce realistic seasonal cycle of the Arctic ML depth.

The MITgcm adjoint code is generated using automatic differentiation tools (Heimbach et al., 2005) Observational constraints used to invert for initial T/S conditions in this study are the final (day 40) hydrography profile measurements. Day-40 model-data misfits are systematically reduced through iterative minimization of a least-square misfit function (adjoint or Lagrange Multiplier method). At each iteration, incremental adjustments are made to uncertain model parameters and input fields (together termed control variables), which are often not well constrained (Fenty & Heimbach, 2012; Forget, et al., 2015a; Stammer, 2005), to bring the model T/S into agreement with the observed hydrography to within data and model representation errors (Forget, Campin, et al., 2015; Nguyen et al., 2017). For this study, the control

variables are the atmospheric forcing inputs: 10-m air temperature, specific humidity, downward long and short wave, precipitation, and 10-m winds.

2-2 Radon deficit method background

The radon deficit is used to determine the air-sea gas transfer velocity (k). The magnitude of k in sea ice zones has been the focus of scientific community in recent years and this method has emerged as one of the promising tools for determining k in sea ice zones (Loose et al., 2017; Rutgers Van Der Loeff et al., 2014). This geochemical method is based on vertical sampling of ^{222}Rn and ^{226}Ra activities (Peng et al., 1979). Both radon and its parent radium are radioactive elements with half-lives of 3.82 days and 1599 years, respectively (Peng et al., 1979). In a closed system, based on the mismatch in their respective half-lives radon and radium reach secular equilibrium, whereby the activity of the daughter (^{222}Rn) is determined exclusively by the activity of the parent (^{226}Ra). When secular equilibrium is reached the activity of radon (A_{Rn}) would match the activity of radium (A_{Ra}). In the deep ocean, away from the surface and the sediments, the secular equilibrium is a valid assumption.

In the surface ocean, the vertically integrated conservation of mass for radon in terms of activities can be written as:

$$\int_0^D \frac{dA_{Rn}}{dt} dz = \lambda \int_0^D (A_{Ra} - A_{Rn}) dz - kA_{Rn}^{surface} - FmM(A_{Rn}^{FmM} - A_{Rn}^{surface}) + Adv + Mix$$

(Eq-1)

where λ is the decay constant of radon (0.181 d^{-1}), D is an arbitrary depth, k is gas exchange velocity ,and FmM is freezing minus melting rate. A_{Rn} and A_{Ra} are radon and radium activities. A^{FmM} and $A^{surface}$ denote the activity in sea ice and water

surface, finally Adv and Mix accounts for effects of advection and mixing. Based on current geochemical approaches, to account for time dependency of a gas budget, a weighted average of k is used (Reuer et al., 2007). For radioactive budgets, these weights are based on fraction of ML that has been ventilated and radioactive decay rate. This weighted average method allows for neglecting the LHS of (Eq-1). Away from sea ice zones, FmM is equal to zero. Vertical mixing leads to rapid air-sea exchange and the lateral differences in gas concentration are assumed negligible from advection i.e. 2 last terms in RHS are negligible. Rapid mixing would results in vertically constant activities in ML and allows us to set D equal to ML depth. Therefore the conservation of mass for radon, near the surface can be simplified to:

$$\left(\frac{A_{Ra}}{A_{Rn}} - 1\right) \lambda H = k$$

(Eq-2)

where A_{Rn} observed activity of radon and A_{ra} is observed activity of radium. Both activity values can be obtained by a single vertical sampling of radon and radium.

We compare the 1D model and its adjoint with in-situ formulations for 53 sampling stations in Arctic Ocean to investigate the influence of process other than air-sea exchange. These sampling stations cover a diverse range of time scale and sea ice conditions (Figure). Samples from ARK-XXVI/3 2011 Sep/Aug (Rutgers Van Der Loeff et al., 2014) and JOIS 2013 Sep/Aug and JOIS 2014 Sep/Oct (Loose et al., 2017), cover late summer and early fall and sea ice conditions that range from open ocean to almost fully covered sea ice.

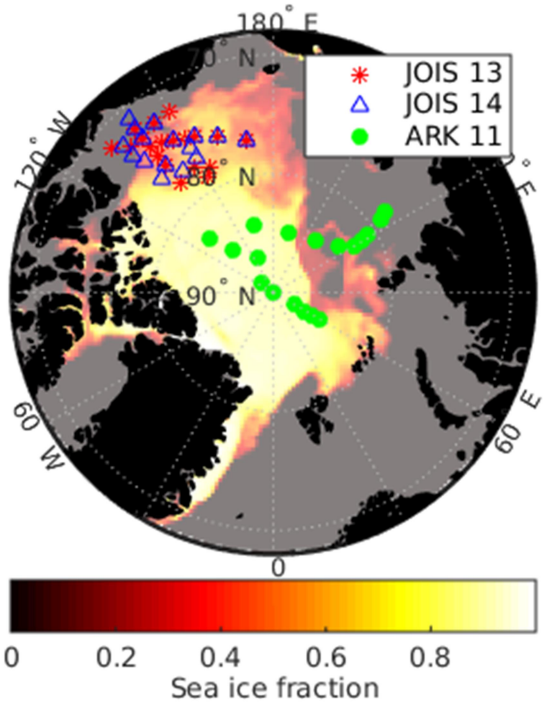

Figure 1 Location of the sampling stations from JOIS 2013, JOIS 2014 ,and ARK 2011. The overlay color map shows the summer minimum sea ice fraction averaged from 2011 to 2014.

2-3 Implication on other biogeochemical gases such as O_2

The calculations offered in this paper are explicitly done for budget of radon, in this section we are going to demonstrate how these calculations can also be applicable to other geochemical gases. We chose oxygen as an example and offer a scaling argument between similar terms in conservation of mass for radon and oxygen. The conservation for oxygen can be written as:

$$\int_0^D \frac{d\,C_{O_2}}{dt} dz = G - R + kC_{O_2}^{Sat} - kC_{O_2}^{surface} - FmM(C_{O_2}^{Fm} - C_{O_2}^{surface}) + Adv + Mix$$

(Eq-3)

where C_{O_2} is concentration of oxygen, G is gross production of oxygen, R is respiration, $C_{O_2}^{Sat}$ is oxygen saturation concentration. In this equation the effects of bubble mediated transport are neglected (Kaiser et al., 2005).

There is a similarity between main sources of uncertainty e.g. advection, mixing, freeze/melt effects in Eq-3 and Eq-1. The possible difference, regarding the uncertainties, between these two equations is the ratio between time scale associated with sources of uncertainty and renewal rate of gas budget in ML (production - consumption). For gas exchange and radon for example a possible scaling is $\lambda \int_0^H (A_{Ra} - A_{Rn})dz$ divided by $k_{Rn}A_{Rn}^{surface}$, for oxygen this scaling can be written as $G - R + k_{O_2}C_{O_2}^{Sat}$ divided by $k_{O_2}C_{O_2}^{surface}$.

First order estimation of the scaling ratio for Rn, based on Eq-2, is approximately one. For O_2, simplification of the terms in the nominator, considering G - R << $k_{O_2}C_{O_2}^{Sat}$ (Reuer et al., 2007), would result in the scaling ratio for O_2 to be equal to $C_{O_2}^{Sat}/C_{O_2}^{surface}$. Therefore, the ratio to translate the magnitude of error, for gas exchange, between O_2 to Rn can be estimated by $C_{O_2}^{Sat}/C_{O_2}^{surface}$. The surface to saturation concentration of O_2 ratio in marginal zones can be estimated at 1.0 ± 0.2 (Eveleth et al., 2014). This number suggests that errors introduced by assumptions in k calculation for O_2 and Rn, although not exactly equal, will have the same magnitude.

The scaling argument offered in this section lead us to believe that the uncertainties that are going to be calculated later on this paper, offer good first guess for errors introduced in other biogeochemical gases. Nevertheless, If the exact errors

are needed be calculated for specific gas, the forward section of the 1D numerical model should be utilized. For this purpose we uploaded the forward section of 1D numerical model setup and a relevant user manual on the public domain.

2-3 The budget of ^{222}Rn and ^{226}Ra in the 1D model

Forty days prior to the sampling date for each station, we initialized the 1D numerical model and simulate the ML depth and SI fraction and using the Japanese 55-year Reanalysis (JRA55) (Kobayashi et al., 2015) as atmospheric forcing. Initial estimates of temperature and salinity of the water column came from either the outputs of a 9 km horizontal resolution 3D Arctic regional model (Bigdeli et al., 2017; Nguyen et al., 2011) or the final observed T/S at each stations; we tested both set of initial conditions and used the set of profiles that yielded the lowest misfits in the final T and S. Radon and radium are inserted in the water column as passive tracers with their respective half-lives. Tracers are initialized assuming secular equilibrium, matching the radium values observed in each sample. Gas exchange is modeled as a sink for radon at the surface and the magnitude of k at the surface is based on a formulation from W92 (Wanninkhof, 1992), H06 (Ho et al., 2006), N00 (Nightingale et al., 2000), S07 (Sweeney et al., 2007) ,and finally W14 (Wanninkhof, 2014):

$$k_{w92} = 0.308\, U_{10}^{2}\, Sc^{-0.5}(1 - f_{ice}) \qquad \textbf{(Eq4)}$$

$$k_{w99} = 0.028\, U_{10}^{3}\, Sc^{-0.5}(1 - f_{ice}) \qquad \textbf{(Eq5)}$$

$$k_{N00} = (0.100\,U_{10} + 0.220\,U_{10}^2)Sc^{-0.5}(1 - f_{ice}) \quad \textbf{(Eq6)}$$

$$k_{H06} = 0.254\,U_{10}^2\,Sc^{-0.5}(1 - f_{ice}) \quad \textbf{(Eq7)}$$

$$k_{S07} = 0.270\,U_{10}^2\,Sc^{-0.5}(1 - f_{ice}) \quad \textbf{(Eq8)}$$

$$k_{w14} = 0.251\,U_{10}^2\,Sc^{-0.5}(1 - f_{ice}) \quad \textbf{(Eq9)}$$

where k is gas exchange velocity, U_{10} is wind at 10 meter above the interface, Sc is the Schmidt number, and f_{ice} is the ice fraction. These formulations suggest a linear relationship between fraction of open water and gas exchange (Butterworth & Miller, 2016; Evans et al., 2015; Prytherch et al., 2017; Takahashi et al., 2009). It is still an open question whether this linear relationship holds (Fanning & Torres, 1991; Loose et al., 2017; Rutgers Van Der Loeff et al., 2014), we further elaborate if these wind speed formulations explain the observed budgets.

Sea ice formation/melt can result in brine/freshwater discharge in the water column, which in turn would deepen/shoal the mixed layer. Our model captures these phenomena. Sea ice cover, on the other hand, acts as a barrier for gas exchange even if formed outside of our numerical domain and advected to the station's location. We input satellite data (Comiso, 2000) as a mask for gas exchange, and this mask does not affect the heat budget of the water column; hence has no effect on ML depth.

The sea ice in our numerical model contains a prescribed concentration of ^{226}Ra equal to 30% of observed ^{226}Ra at the surface, but the ^{226}Ra 'trapped' in sea ice is only released when the ice melts into the surface ocean. This value of 30% of surface ^{226}Ra is based on ice core samples gathered by Loose et al., (2017). The Ra

and Rn in our simulation can reach secular equilibrium inside the ice and then during the melt/freeze of sea ice, dilution/concentration of Ra and Rn are captured in the surface water.

3-Results

3-1 Optimization

The term t_f is the time in days when mixed layer was sampled for radon and radium, and we anticipate that the hydrographic trajectory of a forward 1D model integration from $t = t_f – 40$ to $t = t_f$ would capture the effect of changes in ML depth on the gas budget, and thus the history of ^{222}Rn over this period. Continuous changes in ML depth have direct impact on the budget of gas available for gas exchange. Thus an accurate representation of the evolution of the ML depth is critical to our ability to quantify a gas budget. In addition to sea ice conditions over the 40 day period, the ML depth evolution depends on the initial density profile at t = tf – 40 and the atmospheric conditions.

In the initial forward 1D model integration, we utilized the outputs from our regional model (Bigdeli et al., 2017) to establish the initial sea ice cover, as well as temperature and salinity in the water column. However, this produced hydrography at $t = t_f$ that was inconsistent with observed T-S profiles from shipboard CTD casts. In a separate test, we have also initialized sea ice cover and hydrography from satellite ice cover and observed hydrography at stations. However, within the 40-day integration period, the evolution of ML depth still diverged from the observed T-S at t = tf. Based

on our previous analysis (Bigdeli 2017), we attribute most of this divergence to poor short-term accuracy in the reanalysis atmospheric conditions.

The observed divergence between 1D model forward runs between t = tf-40 and t = tf, revealed that more effort was necessary to adequately capture the history of ^{222}Rn in the ML. Taking advantage of the adjoint capability in the MITgcm and in the 1-D configuration (Nguyen et al., 2017), we optimized for the initial hydrographic conditions using the observed T-S at $t = t_f$ and observed satellite ice concentration as constraints.

At each station, for each observed T-S profile at $t = t_f$, we assigned a corresponding uncertainty. The uncertainty for T (σ_t) and S (σ_s) are vertically constant profiles equal to 0.1 and 0.5 respectively. These uncertainty values are estimated from maximum variability observed between three CTD casts on the sampling stations. The objective of the optimization is then to estimate an initial T/S profiles ($t = t_{f-40}$) such that hydrographic conditions at $t = t_f$ are within the prescribed uncertainty. In other words, the adjoint optimization aims to minimize the misfit function J:

$$J = J_T + J_S = (T_{obs} - T_{model})^2/\sigma_T^2 + (S_{obs} - S_{model})^2/\sigma_S^2$$

(Eq10)

In the unconstrained forward runs, the misfit J_T and J_S as defined above were 53.80 and 22.84, respectively, when averaged over 53 stations. The optimization reduced the average J_T and J_S to 13.3 and 6.3 through adjustment of uncertain surface atmospheric conditions and initial T and S at $t = t_{f-40}$ (Forget, et al., 2015a; Nguyen et al., 2017). For full convergence, J should be reduced to 1, i.e., T-S misfits fall within

the uncertainty of the observed profiles. However, due to other unknown factors such uncertainty in our estimated σ_T, σ_S and in the atmospheric forcings, J does not reach full convergence here. However, the improvement in the model T and S at tf is significant (75% and 72% respectively) and demonstrates the effectiveness of the optimization procedure (Figure 2).

Station CB-2a is shown (Figure 2) as an example of this optimization process, where the unconstrained run's misfit J_S was significantly higher at 98. After 50 iterations the optimized solution's J_S is reduced to 8 (Figure 2-b). The optimization process, by varying the near surface heat budget, can indirectly effect the evolution of sea ice cover (Figure 2-d). Although there are no direct cost (J) related to ice cover, we did not observe more than 30% divergence of ice cover from satellite data. This value is close to 20% uncertainty reported for satellite data (Ivanova et al., 2015).

Again, the only metric in water column available to us is the ML depth of ~6 meters from CTD at time of sampling $t = t_f$. While the unconstrained model shows stratification up to the surface, the optimized ML depth is ~7 meters, which is consistent with the observation. This improvement is crucial in studying near surface radon budgets. The corresponding optimized ML depth evolution is shown in Figure 2-c. Utilizing the optimized ML depth evolution, we proceed to estimate the near surface radon budgets and investigate the effect of the environmental forcings on these budgets.

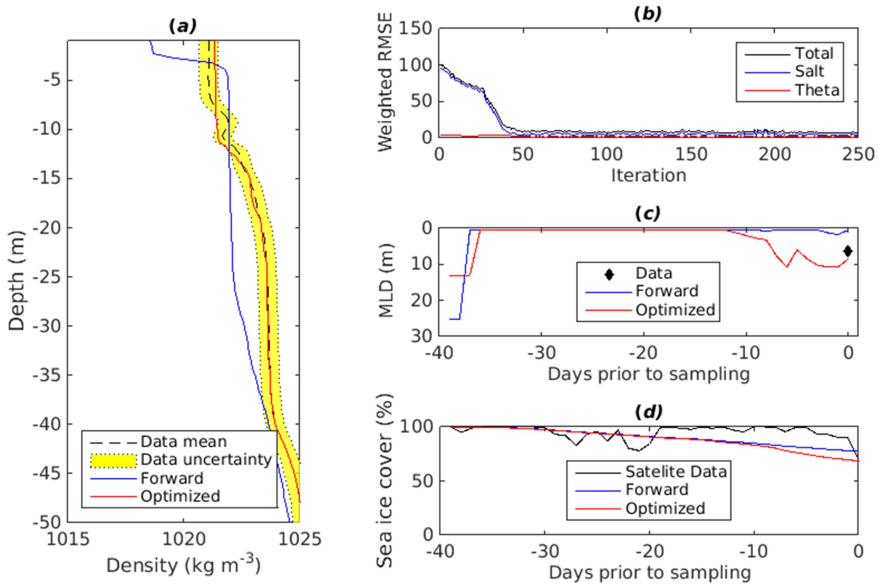

Figure 2 **(a)** Vetical density profiles from CTD cast, forward simulation and optimized run at station CB2-a during JOIS 2013 cruise. **(b)** Weighted root-mean-square error between final salt, temperature and total and CTD data for each iteration of optimization **(c)** Evolution of mixed layer depth for 40 days prior to sampling, blue and red solid line show forward and optimized model outputs and diamond marker show the ML depth from sampling at day 0 i.e. sampling day (**d**) Sea ice cover in (%) for 40 days prior to sampling, blue and red lines show forward and optimized simulated ice cover, black line show sea ice cover from satellite.

3-2 Radon budgets and environmental forcings

With atmospheric forcing and initial conditions optimized, we can move to assessment of environmental forcing effects on radon's budget. This task is divided into two steps. First, we statistically compare the simulated budget with available data; next we quantify the contribution of each forcing on the simulated budgets or radon.

3-2-1 Model results and data: gas exchange parametrization in sea ice zones

In this section we compare the modeled radon budgets with the profiles of radon deficit from the 53 sampling stations. As an example, we showed the results of a 40-day forward integration for two stations in Supporting-information-1. Station CB-27 from the JOIS cruise in 2014 (S-1) and station CB-19 from the JOIS cruise in 2013 (S-2). These two stations show when the model successfully predicts the profile and when it is unsuccessful. The evaluation of each gas exchange formulation, introduced in section 2-2, will be based on how close the simulated ^{222}Rn budgets are to the observed budgets on the sampling day (t_f). For purpose of this comparison, we removed stations that could have had more than 10% error from advection. This criterion removes 10 stations out of 53 and leaves 43 stations in our statistical analysis.

We observed a peculiar case regarding surface values of radon on 4 of our summer stations. During sea ice melt, fresh water with low concentrations of Ra and Rn would be released into the surface water (Loose et al., 2017). Although our model captures these phenomena, we had no information of Ra concentration of surface water when the ice is formed on the last freezing season, we can only estimate the initial Ra values of sea ice based on the observed values of Ra at sampling stations. Even considering the range of Ra across all stations (10 to 18) we cannot explain a phenomenon that is observed in 4 of our summer stations, in which the surface water experiences an increase in concentration of Ra during the melt. One explanation for this phenomenon may be the release of shelf sediments that were entrained into sea ice during the time of ice formation (Notz and Worster, 2009).Further sampling of ice cores may lead to answers regarding why this increase happens instead of the expected dilution.

Our statistical analysis showed formulations of W92, W99, N00, H06, S07, and W14 are bounded by data error bars for ~50% of the stations and we found no statistically significant difference between their results. We showed the result from W14 in Figure 3. The data consistently show higher observed deficits with +80% ice covers, with more than 70% of data landing on positive side of the graph, supporting enhancement of gas exchange beyond the linear scaling in this range of ice covers.

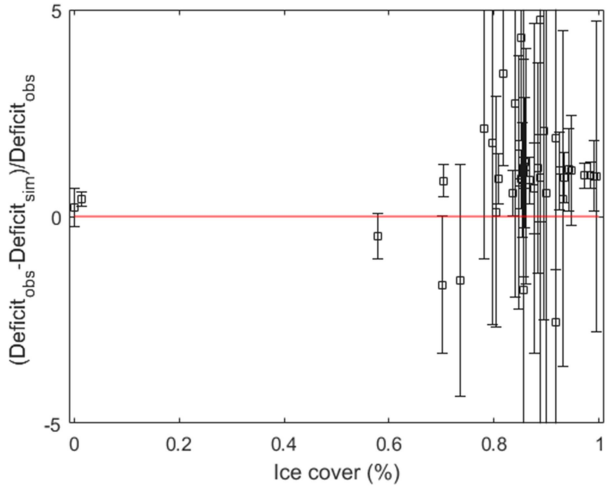

Figure 3 Ratio of budgets simulated with W14 formulation and radon data vs ice cover, the red line show 100% accuracy.

3-2-2 Errors introduced by simplifying assumptions in the geochemical budget

As we stated in the introduction, the common convention is to neglect effects of freeze/melt, mixing and assuming a steady state when interpreting mixed-layer budgets of e.g. oxygen and radon. To quantify the error introduced by each assumption, we should compare the corresponding terms neglected in main

conservation of mass equation (Eq-1). Discretizing Eq-1 in time, we neglect the advection term for now and we denote the vertical integral of the activity (A) to some depth (D) as the budget (B). Finally, if D is allowed to vary in time we arrive at discrete 1D mass conservation of the budget with no further assumptions:

$$\frac{\Delta B_{Rn}}{\Delta t} = \lambda B_{Ra} - \lambda B_{Rn} - kA_{Rn}^{surface} - FmM\left(A_{Rn}^{FmM} - A_{Rn}^{surface}\right) + \frac{\Delta D}{\Delta t}\left(A_{Rn}^{D+\delta D} - A_{Rn}^{D-\delta D}\right) \qquad \text{(Eq11)}$$

where every term on RHS, except the first term, is a function of time. The budget of radium (B_{Ra}) can be treated as steady state in the water column, because sedimentary sources are not proximal (Kadko and Muench, 2005) and the half-life of ^{226}Ra is 1599 yrs. By numerically integrating (Eq-11) forward from secular equilibrium, with a constant D below ML depth (D >> H), using surface Rn and FmM values from the numerical 1D model, and 1 hour time steps, we reach budgets predicted by the 1D numerical model with 10^{-3} accuracy.

To investigate the error that is introduced through the simplifying assumptions in the conventional upper ocean radon budget (e.g. Loose et al., 2017), we evaluate Eq-1 using 1D model output while neglecting the terms correspondent to each assumption. Specifically, we investigate the effect of 1) neglecting ice formation and melt (hereafter called No Freeze/Melt), 2) ignoring the effects resulted from changes in mixed layer depth (Const ML) and 3) using weighted average k (Const k). Finally we also investigate 4) Assuming Steady State condition (Steady State), the latter condition is the combination of all assumptions leading to Eq.2.

The No Freeze/Melt and Const K calculations are straight forward. For No Freeze/Melt, we set FmM equal to zero. For Const k, we compute the Rn budget (B_{Rn}) predicted by weighted average k (Bender et al., 2011; Loose et al., 2017; Reuer et al., 2007; Rutgers Van Der Loeff et al., 2014) to the exact budgets at the end of integration. Const ML depth (H) assumption affects 3 terms in Eq11, first limiting the integral depth (D) to H. Second replacing $A_{Rn}^{surface}$ as B_{Rn} divided by H for each time step, and finally setting the time depend term on RHS ($\frac{\Delta H}{\Delta t}$) to zero. There are no assumption corresponding to time varying ML. Since by adding a time dependency to ML, instead of simplifying the problem, further complications would arise due to lack of information regarding Rn activities in vicinity of ML at each time step ($A_{Rn}^{H+\delta H}$ and $A_{Rn}^{H-\delta H}$). Finally for steady state condition, we apply all these assumptions simultaneously. With these assumption mathematically defined, we move to quantifying the effects of advection.

In some oceanographic circumstances (e.g. in an oligotrophic gyre or far from boundary currents), the assumption of horizontal homogeneity may be more applicable. However in marginal sea ice zones, the lateral gradient of mixed layer depth (Timmermans et al., 2017) and sharp changes in the rate of air-sea flux for heat/momentum/gas due to sea ice cover (Fanning & Torres, 1991) produce significant lateral variations in the surface ocean. The 1D version of the MITgcm does not permit us to capture the effects of advection, but we have developed a simple relationship to capture the effects of lateral heterogeneity. To take into account the horizontal advection of radon we can follow a water parcel that enters our domain from a

hypothetical neighboring cell, effectively adopting a Lagrangian framework for that specific parcel.

Following a hypothetical parcel as it enters the numerical grid cell, we make two simplifying assumptions. First, the environmental forcing including wind, k and FmM are the same between the numerical cell and the traveling parcel. Second, we can estimate $A_{rn}^{surface}$ as B_{rn} divided by H, where H is the same for the traveling parcel and the numerical cell. In other words, we assumed all deviations from horizontal homogeneity are sea ice related, hence every other forcing can be assumed horizontally constant. With this set of assumptions, Eq10 can be used for traveling parcel as well, although, the specific solution to this equation will be dependent on integration time and initial radon budgets.

When solving Eq11 for the numerical cell, we integrate 40 days forward from secular equilibrium i.e. $B_{Rn}^{IC} = B_{Ra}$. In contrast, we have to estimate the initial Rn budget (B_{Rn}^{IC}) and time span of integration for the traveling parcel. The integration time can be simply estimated by dividing the length of the numerical cell (4 km) by the magnitude of Ekman transport (Cole et al., 2014). Initial budgets (B_{rn}^{IC}) were estimated to be related to ice cover. Ice covers at neighboring cells are obtained by finding the minimum and maximum ice cover from satellite data within a circular region centered at observed station location with a radius of 2 km (i.e horizontal spacing of our numerical cell).

This estimation effectively takes into account the balance between the parcels with high/low radon content coming from high/low ice cover and the time it takes for

these parcels to equilibrate compared with the parcels inside the numerical cell. We should note that this method gives an upper limit for effects of advection. By limiting the integration time to the length of the numerical cell divided by Ekman transport, we effectively assumed a straight path for the trajectory of the traveling parcel.

We systemically quantified the error introduced by each of the estimations mentioned above for 53 sampling stations. The errors from No Freeze/Melt, Const ML, Const K, and Steady State are sensitive to ice cover (Figure 4). At the open ocean limit, none of the assumptions result in more than 10% error, the assumption of constant ML depth results in only 5% error. This value is consistent with the 20% error estimated by Bender et al. (2011). These results support the validity of these assumptions in the open ocean limit. The most error from these assumptions, except error from neglecting advection which is only a function of the distance to the ice front, occurs at 10-80% ice cover range.

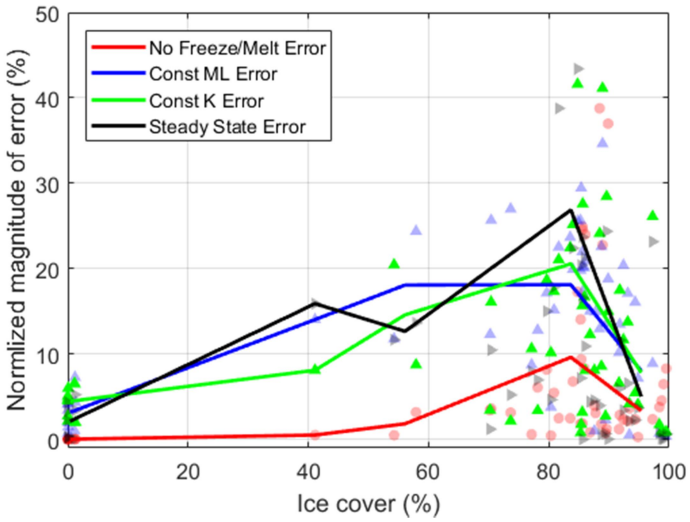

Figure 4 Normlized magnitude of error introduced by neglecting melting/freezing, assuming constant ML, constant k and steady state condtion vs ice cover in % for 53 stations.

We depict the error distribution in the collection of 53 radon deficit stations, using histograms. For example, ignoring the processes of sea ice freeze/melt (Figure 5-b) leads to less than 10% error on 85% of stations and more than 20% accuracy on only 5% of stations, making this assumption a safe estimate. On the other hand, neglecting advection (Figure 5-a) has more than 90% accuracy on 80% of stations but can also generate up to 90% error. This kind of error distribution, when left unresolved, would make interpretation of any budget unreliable. The method offered here assists in filtering out the stations that are susceptible to effects of advection.

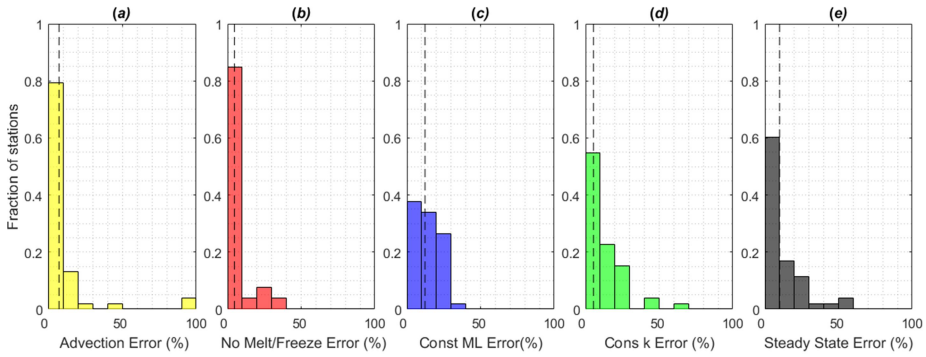

Figure 5 (a-e) fraction of stations binned based on the error of estimation , with dashed line showing the average error for (a) neglecting advection (b) neglecting freeze/melt (c) assuming constant ML (d) assuming a constant k (e) assuming steady state condition

Assuming weighted average k (Figure 5-d) and steady state (Figure 5-e) accurately predicts (<10% error) less than 60% of stations and may result in more than 50% error. Although these methods are valid in open ocean, with less than 10% error (Figure 4), rapid evolution of environmental forcing in marginal ice zones make these assumptions erroneous.

The error associated with assumption of constant ML (Figure 5-c) is mainly, but not entirely, dependent on ML rate of change. This dependency can be less pronounced if ML depth varies with high frequency compared to gas residence time and gas concentration in water below the ML are close to ones inside the ML. These conditions would allow us to estimate surface concentration from combination budget and ML, although with possibility of 40% error.

We have shown the effects the freeze/melt can be neglected with good accuracy and offered a method to filter samples that may have been affected by advection. Mathematically by vertically integrating to a constant depth bellow the ML,

the effects of mixing are also removed from the conservation of mass equation. So if the environmental forcing such as sea ice cover and k is known in conservation of mass equation, is it still necessary to use the 1D numerical model to accurately predict the gas budgets? The answer lies with the estimation of surface concentration of the dissolved gas. The one downside of using the discretized vertically integrated conservation of mass is that it offers no insight in the vertical distribution of concentration. This distribution, hence the surface concentration, is dependent on evolution of ML and exact concentrations around the edges of ML at each time step. Without the 1D numerical model, there no robust way to estimate the surface value from the integrated budget.

Summary and Conclusion

We utilized an optimized 1D numerical model to explain radon profiles observed during three Arctic cruises (n = 53). The optimization based on inversion model reduced the uncertainties in initial conditions and supported the 1D model in capturing the changes in mixed layer depth.

After resolving the environmental forcing and removing the stations affected by advection, we showed current formulation of gas exchange under predict the radon deficit observed in marginal ice zones.

We offered a simple analytical approach to estimate the errors caused by advection and evaluated the accuracy of current assumptions and estimations of near surface gas budgets in sea ice zones. We showed that assumption of constant mixed

layer depth would introduce up to 40% error in estimating near surface gas budgets and importance of resolving this environmental forcing.

References

Abelmann, A., Gersonde, R., Knorr, G., Zhang, X., Chapligin, B., Maier, E., … Tiedemann, R. (2015). The seasonal sea-ice zone in the glacial Southern Ocean as a carbon sink. *Nature Communications*, *6*, ncomms9136. https://doi.org/10.1038/ncomms9136

Acreman, D. M., & Jeffery, C. D. (2007). The use of Argo for validation and tuning of mixed layer models. *Ocean Modelling*, *19*(1–2), 53–69. https://doi.org/10.1016/j.ocemod.2007.06.005

Adcroft, A., Hill, C., Campin, J.-M., Marshall, J., & Heimbach, P. (2004). Overview of the formulation and numerics of the MIT GCM. In *Proceedings of the ECMWF seminar series on Numerical Methods, Recent developments in numerical methods for atmosphere and ocean modelling* (pp. 139–149). Retrieved from http://gfdl.noaa.gov/~aja/papers/ECMWF2004-Adcroft.pdf

Bates, N. R., & Mathis, J. T. (2009). The Arctic Ocean marine carbon cycle: evaluation of air-sea CO2 exchanges, ocean acidification impacts and potential feedbacks. *Biogeosciences*, *6*(11), 2433–2459. https://doi.org/10.5194/bg-6-2433-2009

Bates, N. R., Cai, W. J., & Mathis, J. T. (2011). The ocean carbon cycle in the western Arctic Ocean. *Oceanography*, *24*, 81–95.

Bender, M. L., Kinter, S., Cassar, N., & Wanninkhof, R. (2011). Evaluating gas transfer velocity parameterizations using upper ocean radon distributions. *Journal of Geophysical Research*, *116*(C2). https://doi.org/10.1029/2009JC005805

Bigdeli, A., Loose, B., Nguyen, A. T., & Cole, S. T. (2017). Numerical investigation of the Arctic ice–ocean boundary layer and implications for air–sea gas fluxes. *Ocean Sci.*, *13*(1), 61–75. https://doi.org/10.5194/os-13-61-2017

Butterworth, B. J., & Miller, S. D. (2016). Air-sea exchange of carbon dioxide in the Southern Ocean and Antarctic marginal ice zone. *Geophysical Research Letters*, *43*(13), 2016GL069581. https://doi.org/10.1002/2016GL069581

Castro-Morales, K., Cassar, N., Shoosmith, D. R., & Kaiser, J. (2013). Biological production in the Bellingshausen Sea from oxygen-to-argon ratios and oxygen triple isotopes. *Biogeosciences*, *10*, 2273–2291. https://doi.org/10.5194/bg-10-2273-2013

Cole, S. T., Timmermans, M.-L., Toole, J. M., Krishfield, R. A., & Thwaites, F. T. (2014). Ekman Veering, Internal Waves, and Turbulence Observed under Arctic Sea Ice. *Journal of Physical Oceanography*, *44*(5), 1306–1328. https://doi.org/10.1175/JPO-D-12-0191.1

Comiso, J. (2000). Bootstrap Sea Ice Concentrations from Nimbus-7 SMMR and DMSP SSM/I-SSMIS. Boulder, Colorado USA: NASA DAAC at the National Snow and Ice Data Center.

Detoni, A. M. S., Souza, M. S. de, Garcia, C. A. E., Tavano, V. M., & Mata, M. M. (2015). Environmental conditions during phytoplankton blooms in the vicinity of James Ross Island, east of the Antarctic Peninsula. *Polar Biology*, *38*(8), 1111–1127. https://doi.org/10.1007/s00300-015-1670-7

Dwivedi, S., Haine, T. W. N., & Del Castillo, C. E. (2011). Upper ocean state estimation in the Southern Ocean Gas Exchange Experiment region using the four-dimensional variational technique. *Journal of Geophysical Research: Oceans*, *116*(C4), C00F02. https://doi.org/10.1029/2009JC005615

Evans, W., Mathis, J. T., Cross, J. N., Bates, N. R., Frey, K. E., Else, B. G. T., … Takahashi, T. (2015). Sea-air CO2 exchange in the western Arctic coastal ocean. *Global Biogeochemical Cycles*, *29*(8), 1190–1209. https://doi.org/10.1002/2015GB005153

Eveleth, R., Timmermans, M.-L., & Cassar, N. (2014). Physical and biological controls on oxygen saturation variability in the upper Arctic Ocean. *Journal of Geophysical Research: Oceans*, *119*(11), 7420–7432. https://doi.org/10.1002/2014JC009816

Fanning, K. A., & Torres, L. M. (1991). ^{222}Rn and ^{226}Ra: Indicators of sea-ice effects on air-sea gas exchange. *Polar Research*, *10*, 51–58.

Fenty, I., & Heimbach, P. (2012). Coupled Sea Ice–Ocean-State Estimation in the Labrador Sea and Baffin Bay. *Journal of Physical Oceanography*, *43*(5), 884–904. https://doi.org/10.1175/JPO-D-12-065.1

Fer, I., Peterson, A. K., Randelhoff, A., & Meyer, A. (2017). One-dimensional evolution of the upper water column in the Atlantic sector of the Arctic Ocean in winter. *Journal of Geophysical Research: Oceans*, *122*(3), 1665–1682. https://doi.org/10.1002/2016JC012431

Forget, G., Ferreira, D., & Liang, X. (2015). On the observability of turbulent transport rates by Argo: supporting evidence from an inversion experiment. *Ocean Sci.*, *11*(5), 839–853. https://doi.org/10.5194/os-11-839-2015

Forget, G., Campin, J.-M., Heimbach, P., Hill, C. N., Ponte, R. M., & Wunsch, C. (2015). ECCO version 4: an integrated framework for non-linear inverse modeling and global ocean state estimation. *Geoscientific Model Development*, *8*(10), 3071–3104. https://doi.org/10.5194/gmd-8-3071-2015

Geilfus, N. X., Carnat, G., Papakyriakou, T., Tison, J. L., Else, B., Thomas, H., … Delille, B. (2012). Dynamics of pCO2 and related air-ice CO2 fluxes in the Arctic coastal zone

(Amundsen Gulf, Beaufort Sea). *Journal of Geophysical Research: Oceans*, *117*, C00G10. https://doi.org/10.1029/2011jc007118

Heimbach, P., Hill, C., & Giering, R. (2005). An efficient exact adjoint of the parallel MIT General Circulation Model, generated via automatic differentiation. *Future Generation Computer Systems*, *21*(8), 1356–1371. https://doi.org/10.1016/j.future.2004.11.010

Heimbach, P., Menemenlis, D., Losch, M., Campin, J.-M., & Hill, C. (2010). On the formulation of sea-ice models. Part 2: Lessons from multi-year adjoint sea-ice export sensitivities through the Canadian Arctic Archipelago. *Ocean Modelling*, *33*(1–2), 145–158. https://doi.org/10.1016/j.ocemod.2010.02.002

Ho, D. T., Law, C. S., Smitth, M. J., Schlosser, P., Harvey, M., & Hill, P. (2006). Measurements of air-sea gas exchange at high wind speeds in the Southern Ocean: Implications for global parameterizations. *Geophysical Research Letters*, *33*. https://doi.org/10.1029/2006GL026817

Ivanova, N., Pedersen, L. T., Tonboe, R. T., Kern, S., Heygster, G., Lavergne, T., … Shokr, M. (2015). Inter-comparison and evaluation of sea ice algorithms: towards further identification of challenges and optimal approach using passive microwave observations. *The Cryosphere*, *9*(5), 1797–1817. https://doi.org/10.5194/tc-9-1797-2015

Kadko, D., & Muench, R. (2005). Evaluation of shelf–basin interaction in the western Arctic by use of short-lived radium isotopes: The importance of mesoscale processes. *DEep-Sea Research II*, *52*, 3227–3244.

Kaiser, J., Reuer, M. K., Barnett, B., & Bender, M. L. (2005). Marine productivity estimates from continuous O2/Ar ratio measurements by membrane inlet mass spectrometry. *Geophysical Research Letters*, *32*. https://doi.org/10.1029/2005GL023459

Kara, A. B. (2003). Mixed layer depth variability over the global ocean. *Journal of Geophysical Research*, *108*(C3). https://doi.org/10.1029/2000JC000736

Kitidis, V., Upstill-Goddard, R. C., & Anderson, L. G. (2010). Methane and nitrous oxide in surface water along the North-West Passage, Arctic Ocean. *Marine Chemistry*, *121*, 80–86. http://dx.doi.org/10.1016/j.marchem.2010.03.006

Kobayashi, S., Ota, Y., Harada, Y., Ebita, A., Moriya, M., Onoda, H., … Takahashi, K. (2015). The JRA-55 Reanalysis: General Specifications and Basic Characteristics. *Journal of the Meteorological Society of Japan. Ser. II*, *93*(1), 5–48. https://doi.org/10.2151/jmsj.2015-001

Large, W. G., Danabasoglu, G., Doney, S. C., & McWilliams, J. C. (1997). Sensitivity to Surface Forcing and Boundary Layer Mixing in a Global Ocean Model: Annual-Mean Climatology. *Journal of Physical Oceanography*, *27*(11), 2418–2447. https://doi.org/10.1175/1520-0485(1997)027<2418:STSFAB>2.0.CO;2

Loose, B., Kelly, R. P., Bigdeli, A., Williams, W., Krishfield, R., Rutgers van der Loeff, M., & Moran, S. B. (2017). How well does wind speed predict air-sea gas transfer in the sea ice zone? A synthesis of radon deficit profiles in the upper water column of the Arctic Ocean. *Journal of Geophysical Research: Oceans*, n/a–n/a. https://doi.org/10.1002/2016JC012460

Losch, M., Menemenlis, D., Campin, J.-M., Heimbach, P., & Hill, C. (2010). On the formulation of sea-ice models. Part 1: Effects of different solver implementations and

parameterizations. *Ocean Modelling*, *33*(1–2), 129–144. https://doi.org/10.1016/j.ocemod.2009.12.008

Marshall, J., Adcroft, A., Hill, C., Perelman, L., & Heisey, C. (1997). A finite-volume, incompressible Navier Stokes model for studies of the ocean on parallel computers. *Journal of Geophysical Research: Oceans*, *102*(C3), 5753–5766. https://doi.org/10.1029/96JC02775

Nguyen, A., Ocaña, V., Garg, V., Heimbach, P., Toole, J., Krishfield, R., … Rainville, L. (2017). On the Benefit of Current and Future ALPS Data for Improving Arctic Coupled Ocean-Sea Ice State Estimation. *Oceanography*, *30*(2), 69–73. https://doi.org/10.5670/oceanog.2017.223

Nguyen, A. T., Menemenlis, D., & Kwok, R. (2009). Improved modeling of the Arctic halocline with a subgrid-scale brine rejection parameterization. *Journal of Geophysical Research*, *114*(C11). https://doi.org/10.1029/2008JC005121

Nguyen, A. T., Menemenlis, D., & Kwok, R. (2011). Arctic ice-ocean simulation with optimized model parameters: Approach and assessment. *Journal of Geophysical Research: Oceans*, *116*(C4), C04025. https://doi.org/10.1029/2010JC006573

Nightingale, P. D., Malin, G. M., Law, C., Watson, A., Liss, P. S., Liddicoat, M. I., … Upstill-Goddard, R. C. (2000). In situ evaluation of air-sea gas exchange parameterizations using novel conservative and volatile tracers. *Global Biogeochemical Cycles*, *14*, 373–387.

Notz, D., & Worster, M. G. (2009). Desalination processes of sea ice revisited. *Journal of Geophysical Research*, *114*. https://doi.org/10.1029/2008JC004885

Ohno, Y., Iwasaka, N., Kobashi, F., & Sato, Y. (2008). Mixed layer depth climatology of the North Pacific based on Argo observations. *Journal of Oceanography*, *65*(1), 1–16. https://doi.org/10.1007/s10872-009-0001-4

Peng, T.-H., Broecker, W. S., Mathieu, G. G., & Li, Y.-H. (1979). Radon evasion rates in the Atlantic and Pacific oceans as determined during the Geosecs program. *Journal of Geophysical Research*, *84*, 2471–2486.

Peralta-Ferriz, C., & Woodgate, R. A. (2015). Seasonal and interannual variability of pan-Arctic surface mixed layer properties from 1979 to 2012 from hydrographic data, and the dominance of stratification for multiyear mixed layer depth shoaling. *Progress in Oceanography*, *134*, 19–53. https://doi.org/10.1016/j.pocean.2014.12.005

Prytherch, J., Brooks, I. M., Crill, P. M., Thornton, B. F., Salisbury, D. J., Tjernström, M., … Humborg, C. (2017). Direct determination of the air-sea CO2 gas transfer velocity in Arctic sea ice regions. *Geophysical Research Letters*, 2017GL073593. https://doi.org/10.1002/2017GL073593

Reuer, M. K., Barnetta, B. A., Bender, M. L., Falkowskib, P. G., & Hendricks, M. B. (2007). New estimates of Southern Ocean biological production rates from O2/Ar ratios and the triple isotope composition of O2. *Deep-Sea Research*, *54*, 951–974.

Rutgers Van Der Loeff, M., Cassar, N., Nicolaus, M., Rabe, B., & Stimac, I. (2014). The influence of sea ice cover on air-sea gas exchange estimated with radon-222 profiles. *Journal of Geophysical Research - Oceans*, *119*, 2735–2751. https://doi.org/10.1002/2013JC009321

Shakhova, N., Semiletov, I., Leifer, I., Salyuk, A., Rekant, P., & Kosmach, D. (2010). Geochemical and geophysical evidence of methane release over the East Siberian

Arctic Shelf. *Journal of Geophysical Research: Oceans*, *115*, C08007. https://doi.org/10.1029/2009jc005602

Smethie, W., Takahashi, T., Chipman, D., & Ledwell, J. (1985). Gas Exchangeand CO2 Flux in the Tropical Atlantic Ocean Determined from ^{222}Rn and pCO_2 measurements. *Journal of Geophysical Research*, *90*, 7005–7022.

Stammer, D. (2005). Adjusting internal model errors through ocean state estimation. *Journal of Physical Oceanography*, *35*(6), 1143–1153.

Sweeney, C., Gloor, E., Jacobson, A. R., Key, R. M., McKinley, G., Sarmiento, J.-L., & Wanninkhof, R. (2007). Constraining global air-sea gas exchange for CO2 with recent bomb 14C measurements. *Global Biogeochemical Cycles*, *21*. https://doi.org/10.1029/2006GB002784

Takahashi, T., Sutherland, S. C., Wanninkhof, R., Sweeney, C., Feely, R. A., Chipman, D. W., … de Baar, H. J. W. (2009). Climatological Mean and Decadal Change in Surface Ocean pCO_2, and Net Sea-air CO_2 Flux over the Global Oceans. *Deep-Sea Research Part II*, *56*, 554–577.

Timmermans, M.-L., Marshall, J., Proshutinsky, A., & Scott, J. (2017). Seasonally derived components of the Canada Basin halocline. *Geophysical Research Letters*, *44*(10), 2017GL073042. https://doi.org/10.1002/2017GL073042

Toole, J. M., Timmermans, M.-L., Perovich, D. K., Krishfield, R. A., Proshutinsky, A., & Richter-Menge, J. A. (2010). Influences of the ocean surface mixed layer and thermohaline stratification on Arctic Sea ice in the central Canada Basin. *Journal of Geophysical Research*, *115*(C10). https://doi.org/10.1029/2009JC005660

Vivier, F., Hutchings, J. K., Kawaguchi, Y., Kikuchi, T., Morison, J. H., Lourenço, A., & Noguchi, T. (2016). Sea ice melt onset associated with lead opening during the spring/summer

transition near the North Pole. *Journal of Geophysical Research: Oceans*, *121*(4), 2499–2522. https://doi.org/10.1002/2015JC011588

Wanninkhof, R. (1992). Relationship between wind speed and gas exchange over the ocean. *Journal of Geophysical Research: Oceans*, *97*(C5), 7373–7382. https://doi.org/10.1029/92JC00188

Wanninkhof, R. (2014). Relationship between wind speed and gas exchange over the ocean revisited. *Limnology and Oceanography: Methods*, *12*(6), 351–362. https://doi.org/10.4319/lom.2014.12.351

Wunsch, C., & Heimbach, P. (2007). Practical global oceanic state estimation. *Physica D: Nonlinear Phenomena*, *230*(1), 197–208. https://doi.org/10.1016/j.physd.2006.09.040

Wunsch, C., & Heimbach, P. (2013). Two decades of the Atlantic meridional overturning circulation: Anatomy, variations, extremes, prediction, and overcoming its limitations. *Journal of Climate*, *26*(18), 7167–7186.

Manuscript III

Wave attenuation and gas exchange velocity in marginal sea ice zone

A. Bigdeli[1], T. Hara[1], B. Loose[1], A. T. Nguyen[2]

Under revision at Journal Geophysical Research

[1]Graduate School of Oceanography, University of Rhode Island, Rhode Island, 02882, U.S.A

[2]University of Texas at Austin, Austin, Texas, 78712, US

Key Points

Air sea gas exchange

Marginal sea ice zones

Wave age

Abstract

The gas transfer velocity in marginal sea ice zones exerts a strong control on the input of anthropogenic gases into the ocean interior. In this study a sea state dependent gas exchange parametric model is developed based on the turbulent kinetic energy dissipation rate. The model is tuned to match the conventional gas exchange parametrization in fetch-unlimited, fully developed seas. Next, fetch limitation is introduced in the model and results are compared to fetch limited experiments in lakes, showing that the model captures the effects of finite fetch on gas exchange with good fidelity. Having validated the results in fetch limited waters such as lakes, the model is next applied in sea ice zones using an empirical relation between the sea ice cover and the effective fetch, while accounting for turbulence the sea ice motion effect that is unique to sea ice zones. The model results compare favorably with the available field measurements. Applying this parametric model to a regional Arctic numerical model, it is shown that, under the present conditions, gas flux into the Arctic Ocean may be overestimated by 10% if a conventional parameterization is used.

1 Introduction

Constraining the magnitude of the gas exchange velocity (k) at the air-sea interface in the Marginal Ice Zone (MIZ) has implications on estimating the fluxes of biogenic and anthropogenic gases such as carbon dioxide (Bates, 2006; Evans et al., 2015; Liss et al., 2004; Smedsrud et al., 2013; Takahashi et al., 2009) and methane (Elliott et al., 2011; Uhlig & Loose, 2017; Wåhlström & Meier, 2014). Gas exchange in the MIZ is complex and the relationship between sea ice concentration and carbon

sink is poorly understood (Parmentier et al., 2013). Depending on how one describes the sea ice effects on gas exchange, either as natural stirrers acting on Arctic surface water or as barriers to wave generation, its role can vary from enhancer to inhibitor of carbon sink. With the Arctic MIZ extent (Strong & Rigor, 2013) and ice thickness both declining (Lindsay & Schweiger, 2015), understanding the relationship between gas exchange and sea ice cover is crucial, because ice cover alters the kinetics of gas exchange (McGillis et al., 2001).

The MIZ is unique compared to the open ocean (Loose et al., 2009; Loose & Schlosser, 2011) both with respect to the naturally fetch limited wave field (Smith & Thomson, 2016) and existence of environmental forcings such as sea ice induced turbulence (Loose et al., 2014; McPhee, 2008). Fetch is the distance in which wind acts on the water surface and produces waves. When the energy of the wave is limited by this distance, the resulting wave field is commonly known as fetch limited.

Previous studies on effects of sea ice concentration on gas exchange reveal a field of study that is actively evolving. The first paper to consider the effects of sea ice used a linear dampener on the open ocean gas transfer velocity (Takahashi et al., 2009). Two recent studies support this approximation (Butterworth & Miller, 2016; Prytherch et al., 2017). However, there are other observations that show enhancement (Else et al., 2011; Fanning & Torres, 1991; Loose et al., 2017) as well as reduction (Rutgers Van Der Loeff et al., 2014) of gas exchange beyond the linear relationship due to sea ice. One possible sea ice effect on gas exchange is surface wave attenuation and reduction of breaking wave induced turbulence in the presence of sea ice.

However, none of these studies explicitly considers such wave attenuation effects, which are the focus of the present study.

In the open ocean, results of numerous experiments (Ho et al., 2016; Ho & Wanninkhof, 2016; Nightingale et al., 2000; Sweeney et al., 2007; Wanninkhof, 1992, 2014; Wanninkhof et al., 2004) have shown that wind speed can explain more than 80% of variability in gas exchange (Wanninkhof et al., 2009). These experiments conclude that gas exchange in the open ocean can be explained by quadratic or cubic formulation based on wind speed, with each experiment offering slightly different constants for their proposed formulation. In the open ocean during a fully developed sea state, the wave field is a function of wind. However, if sea state is not dependent on just wind speed, such as within the MIZ, these formulations may lose their validity.

There have been theoretical studies suggesting k is related to wave field (Woolf, 2005; Zhao & Toba, 2001; Zhao & Xie, 2010) although such frameworks are not readily applicable in open ocean (Shuiqing & Dongliang, 2016). Here, we take advantage of the previous studies that suggest turbulence regulates gas exchange in the interface (Lamont & Scott, 1970), and specifically the relationship between the Turbulence Kinetic Energy (TKE) dissipation rate and gas exchange (Katul & Liu, 2017; Lorke & Peeters, 2006; Zappa et al., 2007). The TKE dissipation rate has been used to study the effects of various environmental forcings of gas exchange in low wind conditions, such as by tides (Zappa et al., 2003) and rain (Ho et al., 1997; Tokoro et al., 2008; Zappa et al., 2009). It is a challenging task to utilize this method when a combination of wind, waves, and other environmental forcings act on the water column at the same time. We accomplish this task by fitting a TKE based gas

exchange parametric model to conventional quadratic formulations in open ocean conditions, and then introducing the effects of fetch limitation and sea ice. The sea ice section includes the gas exchange model of Loose et al., 2014 that uses sea ice velocity and floe size distribution as diagnostic variables for gas transfer velocity.

We assess the performance of the parametric model in comparison to conventional formulation in the open ocean, fetch limited seas, and marginal sea ice zones. Furthermore, for investigating the broader impact of this work in realistic settings, the formulation developed in this paper alongside the conventional quadratic model is applied to a numerical model of Arctic Ocean to study the spatial and temporal changes of the gas exchange velocity, which may have been overlooked by the conventional formulas. In section 2, we introduce the formulation and method we use to construct the parametric model. In section 3.1 to 3.3; we compare the model results to available data in the open ocean, fetch limited seas and marginal ice zones. Finally, in section 3.4; we apply the parametric model alongside a conventional gas exchange formulation to a regional general circulation model and in section 4 we summarize our findings.

2 Methods

The model introduced in this manuscript is based on the relationship between the TKE dissipation rate (ε) in water and the gas exchange velocity k (Lamont & Scott, 1970),

$$\boldsymbol{k = \alpha(\nu\varepsilon)^{1/4}\, Sc^{-0.5}},$$ **(Eq-1)**

where α is a constant, ν is the kinematic viscosity, and Sc is the Schmidt number. *Zappa et al.* (2007) suggests that α is equal to 0.419 and we adopt this value in this study as well.

When subjected to wind and waves, ε in the water column can vary vertically. Previous studies suggest that the vertical profile of ε can be divided into 3 regimes. About 10 times the significant wave height (H_s) below the interface, the law of the wall applies, hence proportionality between ε and z^{-1} is observed, where z is the distance to the interface. Closer to the interface, in the region between 10 to 2 times H_s, the effects of wave breaking shift the profile to z^{-2} (Terray et al., 1996). Recently, it has been shown that above the z^{-2} layer, in less than two significant wave heights below the interface, another layer of z^{-1} proportionality exists (Gemmrich, 2010; Sutherland & Melville, 2015). The latter study shows the relationship between ε and z can be written as,

$$\varepsilon = 21\left(c_p/U_{10}\right)^{3.5} u_{*w}^3/\kappa z\ ,$$ (Eq-2)

above the depth of about $0.3H_s$ where c_p is the wave phase velocity at the wave frequency spectral peak, u_{*w} is the friction velocity in water, U_{10} is wind speed at 10 m, and κ is the von Karman constant. The air friction velocity (u_{*a}) is related to U_{10} such that $(u_{*a}/\ U_{10})^2$ is the air sea drag coefficient. The ratio c_p/u_{*a} is often called "wave age".

The main challenge in utilizing Equation-2 is determining the depth at which ε is evaluated, hereafter called z_*. We achieve this empirically, by matching the value of k determined from a combination of Equation-1 and Equation-2, to the existing empirical quadratic formulations of (*Wanninkhof*, 1992; *Nightingale et al.*, 2000; *Ho et al.*, 2006; *Sweeney et al.*, 2007; *Ho and Wanninkhof*, 2016). Most of these quadratic formulations are based on open ocean data, such as GasEx experiment (McGillis et al., 2001) in North Atlantic, in a fully developed sea with wave ages of 29 to 32 (Shuiqing & Dongliang, 2016). We set the value of z_*, such that the resulting k from Eq-1 and Eq-2 is equal to the quadratic formulation of (Ho et al., 2006) (Southern Ocean GasEx) at wave age of 32 which has been observed in same region (Sahlée et al., 2012). Here, we use the COARE 3.5 drag coefficient (Edson et al., 2013) to relate the 10 meter wind speed and the wind friction velocity. The drag coefficient is assumed independent of wave age, since its dependence on wave age is not well understood or constrained (Edson et al., 2013). In Section 3.2 we will show that our main results are not affected significantly even if different sea state dependent drag formulations are introduced instead.

This exercise yields z_* values that decrease with wind speed, from 3 m at wind speed 2 m/s to 10^{-3} m at wind speed 15 m/s. This rapid decrease of z_* is expected because Eq-1 suggests that ε should be proportional to $(U_{10})^8$ to be consistent with the quadratic formulations of k, but Eq-2 suggests ε is proportional to only u_{*w}^3 if z_* is independent of wind speed and the wave age is fixed. This suggests that z_* is not related to the actual depth where the gas exchange process is controlled, as long as we assume that k and epsilon are averaged over some long period of time. This is not surprising

considering the fact that near surface turbulence is often dominated by intense but infrequent wave breaking events, and that time averaged ε and time averaged k are affected by such events in very different ways. We should therefore interpret z_* as a tuning parameter to relate the two well established relationships Eq-1 and Eq-2 and the observed quadratic formulation of k.

In order to estimate the k using Equations 1 and 2 in fetch limited conditions, such as in the MIZ, we need to estimate the wave age c_p/u_{*a}. The relation between the wave age and the fetch is estimated based on the empirical formulation offered in Coastal Engineering Manual (Resio et al., 2002):

$$T_c = 2.398\frac{u_{*a}}{g}\ 10^2 \qquad \text{(Eq-3)}$$

$$T = 0.751\left(\frac{u_{*a}}{g}\right)\left(\frac{xg}{u_{*a}^2}\right)^{-0.33} \quad for\ T < T_c \qquad \text{(Eq-4)}$$

$$T = T_c \qquad for\ T \geq T_c \qquad \text{(Eq-5)}$$

where g is gravitational acceleration, x is the fetch. This empirical formula outputs the wave period (T) at the spectral peak. The phase speed c_p at the spectral peak is then determined using the deep water dispersion relation. This formulation produces wave

ages up to 38 for the open ocean and does not produce older seas (wave age > 40). The relation between fetch, wind speed and wave age is depicted in Figure -a.

We assume that fetch in sea ice zones is related to fraction of sea ice cover by the formulation offered by *Smith and Thomson* (2016)

$$x = 162\, f_{ice}^{-0.49} U_{10}^2 / g$$

(Eq-6)

where f_{ice} is fraction of ice cover between 0 and 1 and x is effective fetch. No upper limit for this formulation is required, because as f goes to 0, x goes to infinity and the wave period goes to T_c.

In addition to the turbulence generated by wind and waves, the near surface turbulence in the MIZ can be further enhanced (diminished) by convection (stratification) and friction around ice floes. These effects are parameterized in the same manner as in *Loose et al.*, (2014). This method contains the effect of buoyant convection/stratification by sea ice freeze/melt (Killawee et al., 1998; Loose et al., 2009) and shear induced by the ice movement (McPhee, 2008).

To assess the spatial and temporal distribution of gas exchange velocity k in realistic settings, the parametric model introduced in this paper, alongside the quadratic formulation offered by *Wanninkhof* (2014), is applied to a regional Arctic model. The Arctic configuration used in this study, which is based on the MITgcm, is described in (Nguyen et al., 2011). Bigdeli et al. (2017) have shown that the model's sea ice velocity, sea ice cover and sea surface temperature are reasonably consistent

with available observations in Arctic. Further details about the numerical model can be found in Supporting Material (S1).

3 Results and discussion

The assessment of wave age gas transfer (hereafter called WAGT) parametric model performance is divided into three steps. First the WAGT model results are compared with open ocean data. Second, the fetch limited formulation of WAGT is assessed using lake data. Third, the data in the MIZ are used to evaluate the WAGT output in ice covered conditions.

3.1 Open ocean

We compare the WAGT output with conventional quadratic parametrizations (Figure -b). The model is tuned to match the parametrization of (Ho et al., 2006) (H06) at the wave age of 32 and it indeed follows that parametrization consistently through all wind regimes. The parametrization of (Wanninkhof, 2014) (W14) is also close to WAGT model at the wave age of 32. The parametrization offered by (Sweeney et al., 2007) (S07) closely follows the WAGT model at the wave age of 34 and (Nightingale et al., 2000) is close to the model at the wave age of 29. All of these wave ages are in the range of fully developed seas.

Typically, wave field information, such as the wave age, is either not recorded or poorly constrained during gas exchange experiments. An exception is the study of *Zappa et al.* (2007), in which the lower and upper bounds of wave age are reported as

12 and 75, respectively. This wide range of wave ages can be attributed to the passing of a storm that has been reported during their sampling. Unfortunately, the wave age at each sampling location was not reported, and was not made available at the time this manuscript was prepared. We therefore compare all the data gathered during that experiment (Figure -c), and note that the observational data are reasonably bounded by the WAGT model results of wave ages 12 and 40. Although the parametric model can be used to estimate k for wave ages higher than 40 if Equation-2 is simply applied, we note that these wave ages are not common in the ocean, only observed during short transient periods, and are beyond the applicability of Equation-2 and the model introduced here.

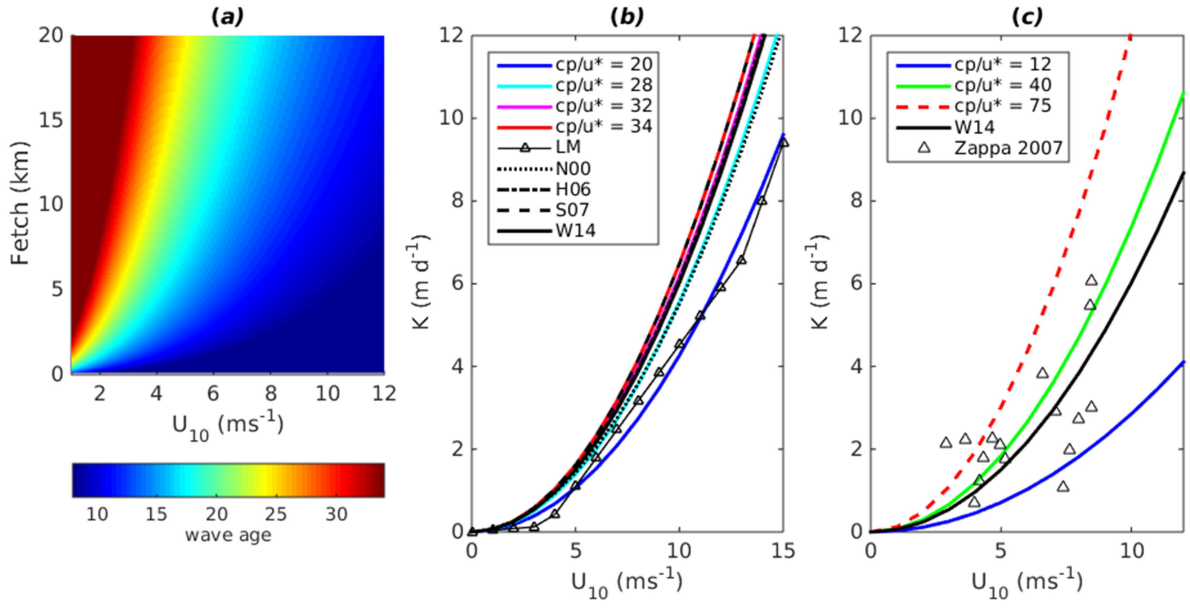

Figure 1 (a) Color map of wave age vs wind speed ms^{-1} vs fetch km. (b) Parameter (WAGT) model gas exchange velocity md^{-1} vs wind ms^{-1} at wave age of 20, 28, 32 and 34, formulation of Liss and Merlivat (LM), Nighttingale (N00), Ho (H06), Sweeney (S07) and Wanninkhof (W14). (c)

Parameter (WAGT) model gas exchange velocity md^{-1} vs wind ms^{-1} at wave ages of 12, 40, and 75 and the data gathered by Zappa in wave ages of 12 to 75.

3.2 Fetch limited experiments in lakes

We next evaluate our model in fetch limited condition with data gathered in Siblyback Lake, Dozmary pool (Kwan & Taylor, 1993; Upstill-Goddard et al., 1991), Rockland Lake, Mono Lake, Crowley Lake (Wanninkhof et al., 1987), and Pyramid Lake (Wanninkhof, 1992). Dozmary Pool, Rockland Lake, and Siblyback Lake have less than 2 km maximum length (from shore to shore). Mono Lake and Crowley Lake have average length of 20 km and Pyramid Lake has maximum length of approximately 50 km.

Due to variant mixing and resident time of tracers employed at each experiment, these datasets have been reported with inconsistent wind speed time averaging blocks. Intercomparison of data necessitate us to compensate the over smoothing of reported wind values. We utilize the empirical formulation offered in Coastal Engineering Manual (*Resio et al.*, 2002):

$$U_t / U_{3600} = 1.5334 - 0.15 \ log_{10} t \qquad \text{(Eq-7)}$$

where t is length of averaging block in seconds. U_t and U_{3600} are wind speed averaged at t seconds and 3600 seconds. With all the wind data transformed into 1 hour averaged blocks, we compare the observational results with our model outputs.

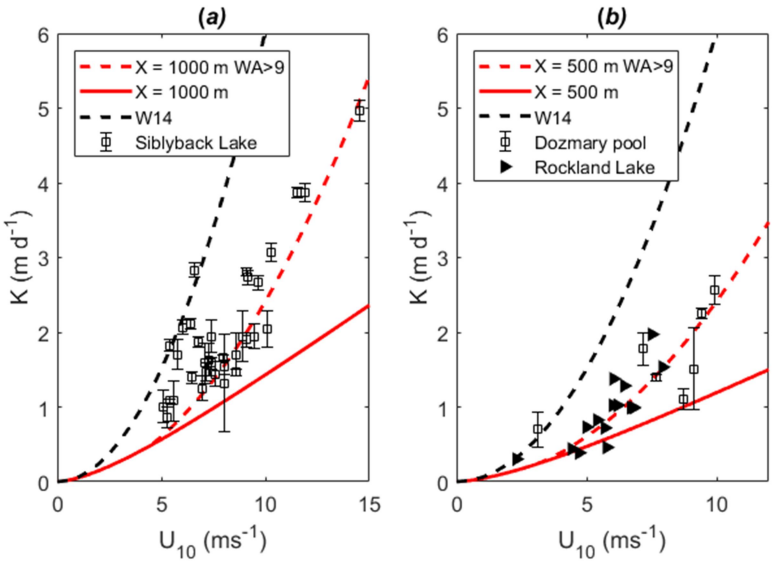

Figure 2 (a) Parameter model gas exchange velocity md^{-1} at fetch limit of 1000 m with (dashed) or without (solid) setting the lower wave age (WA) limit of 9, formulation of Wanninkhof (W14) and data by Upstill-Goddard in Siblyback Lake. (b) Parameter model gas exchange velocity md^{-1} at fetch limit of 500 m with (dashed) or without (solid) setting the lower wave age (WA) limit of 9, formulation of Wanninkhof (W14) and data in Dozmary Pool and Rockland Lake.

With different fetch limits (lake sizes), the modeled gas exchange velocity starts as a single quadratic shape at lower wind speeds (because the wave field is fully developed and is independent of fetch), and then switches to a nearly linear form when the wave field becomes fetch limited at higher wind speeds. The wind speed where this transition takes place increases as the fetch increases. As the wind speed increases further, there is a second transition point where the wave age becomes 9. At wave age 9, the turbulence enhancement coefficient, that is, $21(c_p/U_{10})^{3.5}$ in Equation-2, reaches unity. It is unlikely that the (averaged) dissipation rate becomes less than the wall layer turbulence value below wave age 9. However, it is unclear whether the gas

transfer velocity becomes also independent of sea states below wave age 9. We therefore consider two scenarios; letting the enhancement coefficient fall below one or introducing the lower bound of 1 for enhancement coefficient (that is, setting the wave age minimum of 9 as lower limit). In the second scenario, below wave age 9, ε and consequently k are no longer sensitive to fetch.

The results of the smaller lakes are compared with WAGT model estimates at fetch 1000 m for Siblyback Lake (Figure 2-a) and 500 m for Dozmary Pool and Rockland Lake (Figure 2-b). The gas exchange velocities are significantly lower than the open ocean parameterization (W14) and are quite consistent with our model estimates. The second scenario (with wave age minimum 9) appears to be more consistent with the data.

Crowley Lake, Mono Lake (Figure 3-a), and Pyramid Lake (Figure 3-b) have more than enough size to demonstrate the effect of fetch without the uncertainty of wave age below 9. Again, the reduction of the gas exchange velocity relative to W14 is consistent with the modeled fetch effect.

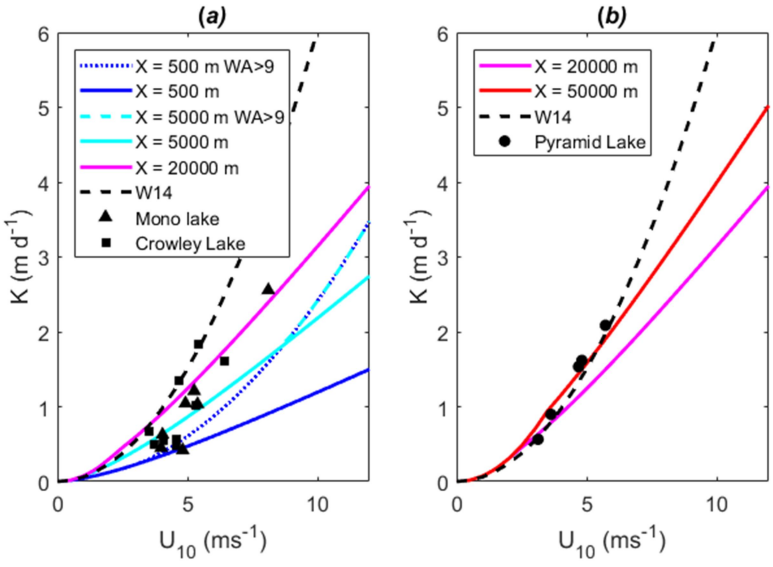

Figure 3 (a) Parameter (WAGT) model gas exchange velocity md^{-1} at fetch limit of 500 m, 5 and 20 km with (dashed or dotted) or without (solid) setting the lower wave age (WA)limit of 9, formulation of Wanninkhof (W14) and data by in Mono Lake and Crowley Lake. (b) Parameter (WAGT) model gas exchange velocity md^{-1} at fetch limit of 20 and 50 km, formulation of Wanninkhof (W14) and data in Pyramid Lake.

There are other fetch limited experiments e.g. in estuaries and laboratories. Wave age estimated in laboratory experiments are less than the threshold of 9 (Bock et al., 1999; P. S. Liss & Merlivat, 1986) and they show a significant sensitivity to drag coefficient (Figure not shown here). Estuaries have enough fetch but are subject to tidal forcing (Borges et al., 2004; Ho et al., 2016). Unresolved sources of turbulence and enhancement of k rule out the possibility of comparison with estuary data. As for the lake results shown here the lines of minimum and maximum modeled gas exchange contain most of the data points, while W14 over-estimates the gas transfer velocity reduction that is caused by fetch limitation.

So far, we have assumed that the drag coefficient is simply a function of wind speed and is independent of sea state. Nevertheless, it is important to consider to what extent our results could be modified if the drag coefficient is dependent on wave age. Previous observations suggest varying degrees of sea state dependence of the drag coefficient (e.g., Edson et al., 2013; Johnson & Vested, 1992; Oost et al., 2002; S. D. Smith et al., 1992) without a clear consensus. For example, Edson et al. (2013) (E13) show very weak sea state dependence, with the normalized roughness length (Charnock coefficient) increasing slightly from 0.013 to 0.031 as wave age decreases from 32 to 8. However, observations by Oost et al. (2002) (O02) indicate much stronger sea state dependence with Charnock coefficient increasing from 0.0066 at wave age 32 to almost 0.1 for wave age below 13. We introduce these two very different sea state dependent drag coefficient formulations, E13 and O02, in our model of the gas transfer velocity, allowing wave age to vary from 32 to 8 (lowest data point available in empirical Eq. 2).

Figure 4-a shows that the drag coefficient can be increased by almost twofold at wave age 8 if O02 is used. However, Figure 4-b shows that the effect of sea state dependent drag coefficient on the transfer velocity is quite weak (compare red dashed line and black dashed line); the transfer velocity at wave age 8 is significantly reduced compared to the fully grown sea (wave age 32) case (black solid line) regardless of the drag coefficient formulations. This is because the transfer velocity is proportional to only 3/8-th power of the drag coefficient (3/4-th power of the friction velocity). These results clearly suggest that the effect of the sea state dependent dissipation rate on gas exchange is much stronger than the possible effect of the sea state dependent drag

coefficient on gas exchange, and that the results of this study are not significantly changed even if different sea state dependent drag coefficient formulations are introduced.

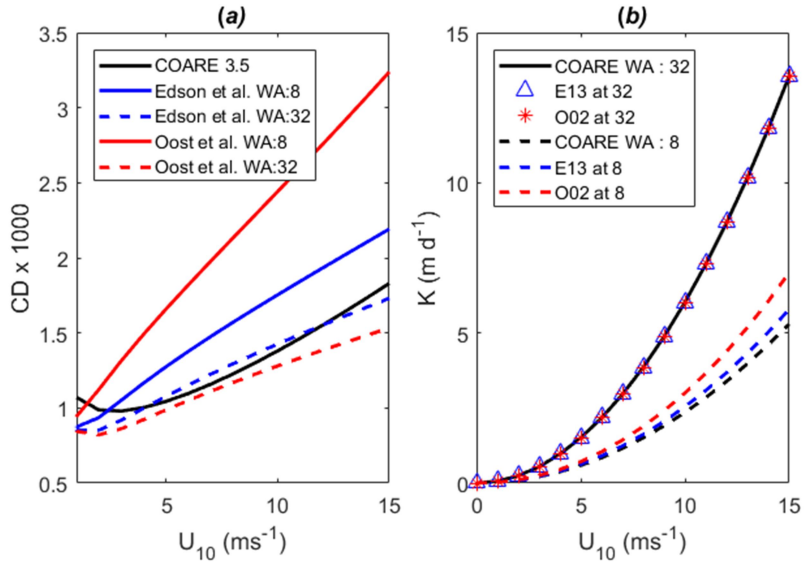

Figure 4 (a) Drag coefficient and (b) gas transfer velocity vs wind speed based on COARE 3.5, Edson et .al (2013 (E13)), and Oost et .al (2002) (O02) drag coefficient formulations at wave age of 8 and 32.

3.3 Sea Ice zones

The equation connecting effective fetch and sea ice is offered by *Smith and Thomson* (2016) during a study on Arctic wave field. This relationship (Eq-6) relates effective fetch with fraction of sea ice to power of -0.49. The wave age goes to 32.2 (Figure 5-a) as the sea ice fraction goes to zero, but it quickly drops to values below 20 with medium sea ice cover and wind speeds.

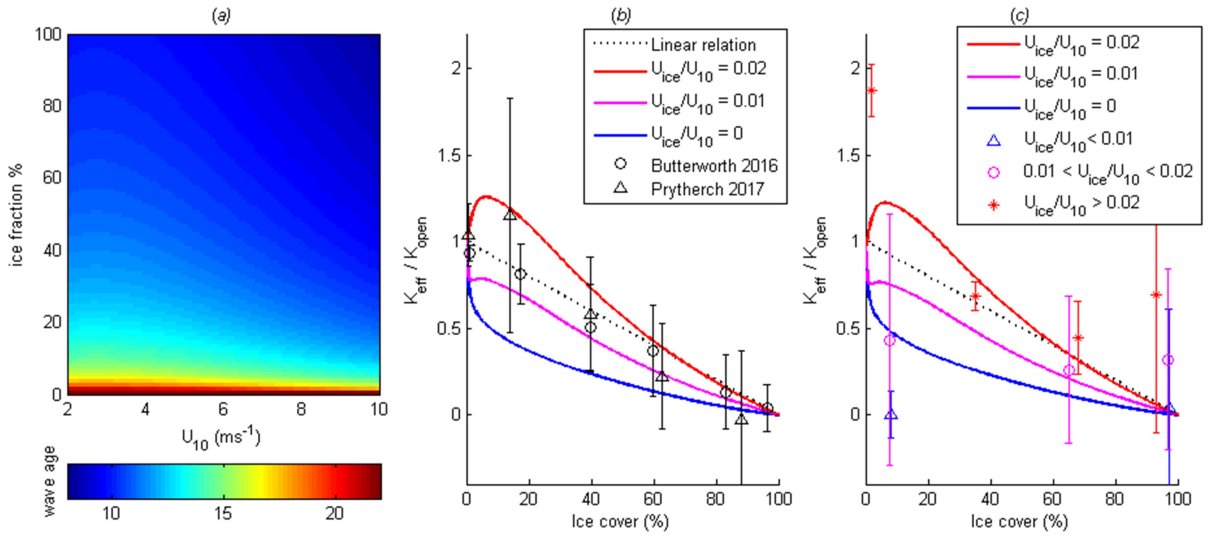

Figure 5 (a) Color map of wave age vs wind speed ms^{-1} vs ice fraction %. (b) Ratio of effective gas exchange over gas exchange in open water vs ice fraction % at U_{10} = 5 ms^{-1}. Solid lines show WAGT model prediction for sea ice speed at 10, 5 ,and 0 cms^{-1}. Eddy covariance data from Butterworth & Miller, (2016) and Prytherch et al., (2017) squares and circles mark the median and error bars show the standard error. (c) Ratio of effective gas exchange over gas exchange in open water vs ice fraction for WAGT model, compared with radon data from Loose et al., (2017) and Rutgers Van Der Loeff et al., (2014). Data are marked with circles, triangles, and starts and are binned based on SI concentration and grouped and colored based on ratio of sea ice to wind speed.

The conventional method regarding the relationship between effective gas exchange (k_{eff}) in ice covered seas and gas exchange in open waters (k_{open}) is to assume a linear relationship between effective gas exchange and fraction of open water in sea ice zones. The linear relationship assumes sea ice as a barrier or lid for gas exchange, forgoing any effect of sea ice dynamics on either wave field or near

surface turbulence. Therefore, this method neglects any wave attenuation or turbulence enhancement by sea ice.

We investigate the effects of fetch dependent wave fields and sea ice motion on k_{eff} in sea ice zones, by normalizing k_{eff} by k_{open}. The effects of sea ice induced turbulence (*McPhee*, 2008) depend on sea ice velocity (U_{ice}). Without any turbulence generation from sea ice ($U_{ice} = 0$), the WAGT model predicts much lower values for effective gas exchange in medium sea ice cover due to wave attenuation (dark blue line in Figure 5-b).

As U_{ice} increases, the sea ice forcing starts to enhance the k_{eff}. Even with this enhancement the k_{eff} from WAGT model remains less than conventional methods until the sea ice velocity gets close to the free drift velocity ($U_{ice} = 0.02\ U_{10}$). With free drifting ice and sea ice covers below 60%, the WAGT model predicts an enhancement of gas exchange beyond the linear relation.

We first compare our model predictions and the eddy covariance data available from (Butterworth & Miller, 2016) and (Prytherch et al., 2017). We compare the k_{eff} to k_{open} ratio for the EC data and WAGT parametric model output (Figure 5-b). The EC data consists of 482 and 612 samples in MIZ for *Butterworth and Miller* (2016) (BM16) and *Prytherch et al.* (2017) (P17), respectively. There is a great variability in these two data sets and the error bars cover both the linear relationship and the WAGT model with free drifting ice. Some of this scatter in the EC data may reflect the influence of processes that we attempt to capture with the WAGT model. The WAGT results with $0.01\ U_{10} < U_{ice} < 0.02\ U_{10}$ mostly bounds the EC data, suggesting that sea

ice drift might account for much of the scattering, however we would require more detail into the ice and water column properties in order to further test the ability of the WAGT model or the linear relationship to reproduce the EC data. In summary, with these data sets both the WAGT and linear model can reproduce the spatially averaged EC data.

We next compare our model with estimates of k by the radon deficit method. Interpreting the radon data in MIZ is rather a complex task. This complexity is due to variability in mixed layer depth and sea ice forcings that are acting on radon budget prior to sampling. Here we simply employ the weighted time average (Bender et al., 2011; Loose et al., 2017) of k as k_{open} for each of n=53 samples (Loose et al., 2017; Rutgers Van Der Loeff et al., 2014) and normalized the k from radon deficit by this weighted k. The details of this procedure can be found in Supporting Material (S2). The results have been binned by sea ice concentration and grouped based on ratio of time averaged ice speed to wind speed (Figure 5-c). The most interesting feature in this comparison is the maximum enhancement observed at ~5% ice cover where both the data and model show enhancement beyond the linear relationship. It is also encouraging that WAGT model predicts very low k values compared to the linear model when sea ice motion is weak (U_{ice} = 0), being consistent with the observations. In summary, the radon method results show somewhat better agreement with the WAGT model than with the linear relationship, since the former may explain the observed large variability of k and its dependence on sea ice drift velocity.

3.4 Arctic Ocean

We apply the WAGT model alongside the formulation from (Wanninkhof, 2014) (K_{w14}) to Arctic regional domain of MIT general circulation model (MITgcm). The outputs of numerical model, including sea ice cover, sea ice velocity, sea surface temperature and salinity, are daily averaged from 2006 to 2012 and then used as an input to the WAGT model. The quantity of interest is the ratio of effective K_{w14} to the effective gas exchange velocity from the WAGT model.

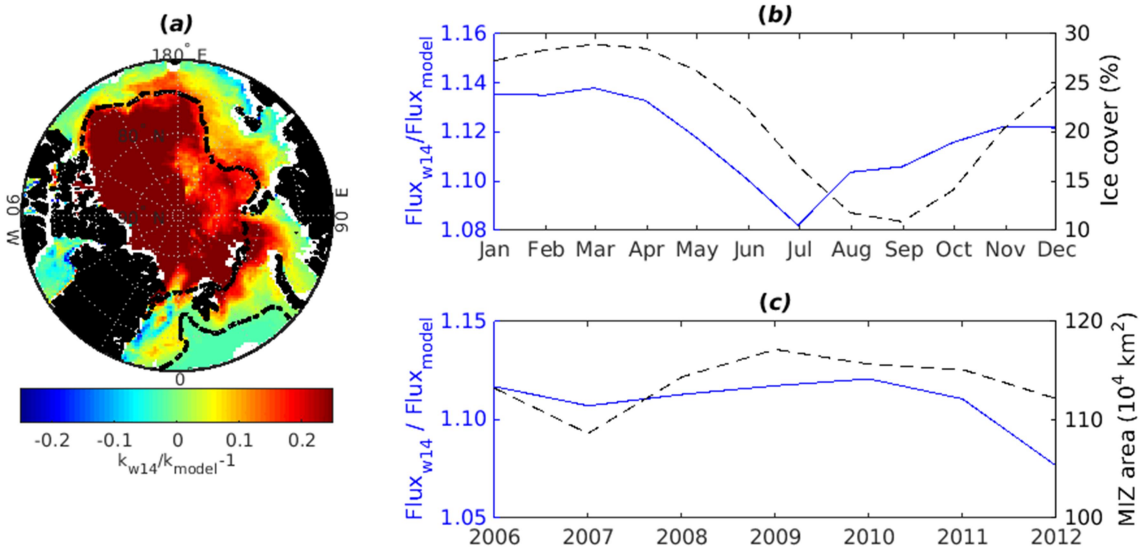

Figure 6 (a) Spatial distribution of the ratio between daily gas exchange velocities based on W14 and WAGT parameter model averaged from 2006 to 2012, dashed lines show averaged ice cover at 10% and 90%. (b) The blue line and left axis depict the ratio of flux over entire Arctic ocean based on W14 and WAGT model, the dashed black line and right axis show the spatially averaged sea ice cover in % , each month is averaged between year 2006 to 2012 . (c) The blue line and left axis are the same as (b) but yearly averaged, the dashed line and left axis demonstrate the sum of areas that have 1 to 99% cover.

First, we investigate the time averaged spatial distribution of the ratio (Figure 6-a). The most pronounced features include overestimation by 20% north of Greenland. With immobile ice cover, such as fast ice or packed ice, the distribution

shows a ratio higher than one such is the case in central Arctic. But when the ice is sparse enough to free drift, the ratio is near one as is the east of Greenland and Arctic peripheries. The distribution shows the ratio of one in ice free regions such as Norwegian Seas.

In order to elucidate the temporal variation of the ratio, the daily flux ratio over entire region north of 70° has been calculated and averaged over 5 years for each month (Figure 6-b), this ratio is independent of partial pressure due to common terms in nominator and denominator. There is an obvious correlation between sea ice cover and the ratio, as the cover increases, the ratio also increases and vice versa, albeit with a lag. This behavior should be viewed from packed ice perspective since areas covered by this type of ice are dominant. As the packed floes start to melt, they start to be more susceptible to wind forcing and gaining higher ice velocity, increasing the denominator of the ratio, hence the ratio minimum in July.

Another aspect of temporal variability is how the ratio would change in response to the area of marginal sea ice zones (MIZ) i.e. areas with more than 1% and less than 99% ice cover from 2006 to 2012 (Figure 6-c). A positive correlation can be found between the ratio and MIZ area. As we move toward the ice free zones and a decrease in sea ice extent, the ratio will get closer to one. Based on the results of the parametric model introduced in this paper, the conventional models may be overestimating the flux into Arctic by 10% in the present climate.

4 Summary and conclusion

We have developed a parametric Wave Age and Gas Transfer (WAGT) model based on the earlier studies relating the turbulence dissipation rate to gas exchange. First, the WAGT model is tuned to match the quadratic formulation in open ocean, when the wave field is fully developed. Next, the fetch (or wave age) effect is incorporated into the WAGT model, and the model is successfully tested against observational data in lakes. Sea ice cover is then introduced in the WAGT model both as a source for turbulence and as an effective fetch limiter. The effect of the sea ice velocity has been investigated and it is shown that, on free drift speed, sea ice generates enough turbulence to overcome the effects of wave attenuation.

Finally, the WAGT model is applied to a regional Arctic ocean-sea ice model. Comparison with the conventional quadratic formulation, with linear relationship with ice cover, shows that the enhancement by sea ice motion is dwarfed by the suppression of wave driven turbulence and consequently, when averaged over 70 degree north, the flux of gases into the Arctic Ocean is overestimated by 10% by conventional formulations in the present climate.

Although our WAGT model is constructed by adding many components, we have so far been able to compare only the combined end result of the gas transfer velocity with existing observations. In the future, it will be desirable to test each model component separately with field and lab data that capture both gas exchange and the forcing, to clarify how different ice related physical processes affect gas exchange.

Acknowledgment

We appreciate the feedback from xx anonymous reviewers. We also acknowledge *high-performance computing support from Yellowstone (ark:/85065/d7wd3xhc) provided by NCAR's Computational and Information Systems Laboratory, sponsored by the National Science Foundation*. *The WAGT model described in this manuscript is available as Open Source and can be accessed via URL:* http://looselab.gso.uri.edu *Funding for this research was provided by the NSF Arctic Natural Sciences program through Award # 1203558.*

References

Bates, N. R. (2006). Air-sea CO2 fluxes and the continental shelf pump of carbon in the Chukchi Sea adjacent to the Arctic Ocean. *Journal of Geophysical Research: Oceans*, *111*(C10), n/a-n/a. https://doi.org/10.1029/2005JC003083

Bender, M. L., Kinter, S., Cassar, N., & Wanninkhof, R. (2011). Evaluating gas transfer velocity parameterizations using upper ocean radon distributions. *Journal of Geophysical Research*, *116*(C2). https://doi.org/10.1029/2009JC005805

Bigdeli, A., Loose, B., Nguyen, A. T., & Cole, S. T. (2017). Numerical investigation of the Arctic ice–ocean boundary layer and implications for air–sea gas fluxes. *Ocean Sci.*, *13*(1), 61–75. https://doi.org/10.5194/os-13-61-2017

Bock, E. J., Hara, T., Frew, N. M., & McGillis, W. R. (1999). Relationship between air-sea gas transfer and short wind waves. *Journal of Geophysical Research*, *104*, 25,821-25,832.

Borges, A. V., Delille, B., Schiettecatte, L.-S., Gazeau, F., Abril, G., & Frankignoulle, M. (2004). Gas transfer velocities of CO2 in three European estuaries (Randers Fjord, Scheldt, and Thames). *Limnology and Oceanography*, *49*(5), 1630–1641. https://doi.org/10.4319/lo.2004.49.5.1630

Butterworth, B. J., & Miller, S. D. (2016). Air-sea exchange of carbon dioxide in the Southern Ocean and Antarctic marginal ice zone. *Geophysical Research Letters*, *43*(13), 2016GL069581. https://doi.org/10.1002/2016GL069581

Elliott, S., Maltrud, M., Reagan, M., Moridis, G., & Cameron-Smith, P. (2011). Marine methane cycle simulations for the period of early global warming. *Journal of Geophysical Research: Biogeosciences*, *116*(G1), G01010. https://doi.org/10.1029/2010JG001300

Else, B. G. T., Papakyriakou, T. N., Galley, R. J., Drennan, W. M., Miller, L. A., & Thomas, H. (2011). Wintertime CO2 fluxes in an Arctic polynya using eddy covariance: Evidence for enhanced air-sea gas transfer during ice formation. *Journal of Geophysical Research-Oceans*, *116*, C00G03. https://doi.org/10.1029/2010JC006760

Evans, W., Mathis, J. T., Cross, J. N., Bates, N. R., Frey, K. E., Else, B. G. T., … Takahashi, T. (2015). Sea-air CO2 exchange in the western Arctic coastal ocean. *Global Biogeochemical Cycles*, *29*(8), 1190–1209. https://doi.org/10.1002/2015GB005153

Fanning, K. A., & Torres, L. M. (1991). ^{222}Rn and ^{226}Ra: Indicators of sea-ice effects on air-sea gas exchange. *Polar Research*, *10*, 51–58.

Gemmrich, J. (2010). Strong Turbulence in the Wave Crest Region. *Journal of Physical Oceanography*, *40*(3), 583–595. https://doi.org/10.1175/2009JPO4179.1

Ho, D. T., Law, C. S., Smitth, M. J., Schlosser, P., Harvey, M., & Hill, P. (2006). Measurements of air-sea gas exchange at high wind speeds in the Southern Ocean: Implications for global parameterizations. *Geophysical Research Letters*, *33*. https://doi.org/10.1029/2006GL026817

Ho, D. T., Bliven, L., Wanninkhof, R., & Schlosser, P. (1997). The effect of rain on air-water gas exchange. *Tellus*, *49B*, 149–158.

Ho, D. T., Coffineau, N., Hickman, B., Chow, N., Koffman, T., & Schlosser, P. (2016). Influence of current velocity and wind speed on air-water gas exchange in a mangrove estuary. *Geophysical Research Letters*, *43*(8), 2016GL068727. https://doi.org/10.1002/2016GL068727

Ho, D. T., & Wanninkhof, R. (2016). Air–sea gas exchange in the North Atlantic: 3He/SF6 experiment during GasEx-98. *Tellus B: Chemical and Physical Meteorology*, *68*(1), 30198. https://doi.org/10.3402/tellusb.v68.30198

Katul, G., & Liu, H. (2017). Multiple mechanisms generate a universal scaling with dissipation for the air-water gas transfer velocity. *Geophysical Research Letters*, *44*(4), 2016GL072256. https://doi.org/10.1002/2016GL072256

Killawee, J. A., Fairchild, I. J., Tison, J.-L., Janssens, L., & Lorrain, R. (1998). Segregation of solutes and gases in experimental freezing of dilute solutions: Implications for natural glacial systems. *Geochimica et Cosmochimica Acta*, *62*, 3637–3655.

Kwan, J., & Taylor, P. A. (1993). A reassessment of the gas transfer velocity — wind speed relationship from the Siblyback Lake data. *Tellus B*, *45*(3), 296–298. https://doi.org/10.1034/j.1600-0889.1993.t01-2-00006.x

Lamont, J. C., & Scott, D. S. (1970). An eddy cell model of mass transfer into the surface of a turbulent liquid. *AIChE Journal*, *16*(4), 513–519. https://doi.org/10.1002/aic.690160403

Lindsay, R., & Schweiger, A. (2015). Arctic sea ice thickness loss determined using subsurface, aircraft, and satellite observations. *The Cryosphere*, *9*(1), 269–283. https://doi.org/10.5194/tc-9-269-2015

Liss, P. S., & Merlivat, L. (1986). *Air–sea gas exchange rates: Introduction and synthesis*. Dordrecht.

Liss, P. S., Chuck, A. L., Turner, S. M., & Watson, A. J. (2004). Air-sea gas exchange in Antarctic waters. *Antarctic Science*, *16*(4), 517–529. https://doi.org/10.1017/S0954102004002299

Loose, B., Kelly, R. P., Bigdeli, A., Williams, W., Krishfield, R., Rutgers van der Loeff, M., & Moran, S. B. (2017). How well does wind speed predict air-sea gas transfer in the sea ice zone? A synthesis of radon deficit profiles in the upper water column of the Arctic

Ocean. *Journal of Geophysical Research: Oceans*, n/a–n/a. https://doi.org/10.1002/2016JC012460

Loose, B., & Schlosser, P. (2011). Sea ice and its effect on CO_2 flux between the atmosphere and the Southern Ocean interior. *Journal of Geophysical Research-Oceans*, *116*. https://doi.org/10.1029/2010JC006509

Loose, B., McGillis, W. R., Perovich, D., Zappa, C. J., & Schlosser, P. (2014). A parameter model of gas exchange for the seasonal sea ice zone. *Ocean Science*, *10*(1), 1–16. https://doi.org/10.5194/os-10-1-2014

Loose, B., McGillis, W. R., Schlosser, P., Perovich, D., & Takahashi, T. (2009). Effects of freezing, growth, and ice cover on gas transport processes in laboratory seawater experiments. *Geophysical Research Letters*, *36*(5), L05603. https://doi.org/10.1029/2008GL036318

Loose, B., Schlosser, P., Perovich, D., Ringelberg, D., Ho, D. T., Takahashi, T., … Tison, J.-L. (2010). Gas diffusion through columnar laboratory sea ice: Implications for mixed-layer ventilation of CO2 in the seasonal ice zone. *Tellus B*, *63*, 23–29. https://doi.org/10.1111/j.1600-0889.2010.00506.x

Loose, B., Schlosser, P., Perovich, D., Ringelberg, D., Ho, D. t., Takahashi, T., … Tison, J.-L. (2011). Gas diffusion through columnar laboratory sea ice: implications for mixed-layer ventilation of CO2 in the seasonal ice zone. *Tellus B*, *63*(1), 23–39. https://doi.org/10.1111/j.1600-0889.2010.00506.x

Lorke, A., & Peeters, F. (2006). Toward a Unified Scaling Relation for Interfacial Fluxes. *Journal of Physical Oceanography*, *36*(5), 955–961. https://doi.org/10.1175/JPO2903.1

McGillis, W. R., Edson, J. B., Hare, J. E., & Fairall, C. W. (2001). Direct covariance air-sea CO_2 fluxes. *Journal of Geophysical Research*, *106*, 16729–16745.

McPhee, M. G. (2008). *Air-ice-ocean interaction: Turbulent ocean boundary layer exchange*. New York: Springer.

Nguyen, A. T., Menemenlis, D., & Kwok, R. (2011). Arctic ice-ocean simulation with optimized model parameters: Approach and assessment. *Journal of Geophysical Research: Oceans*, *116*(C4), C04025. https://doi.org/10.1029/2010JC006573

Nightingale, P. D., Malin, G. M., Law, C., Watson, A., Liss, P. S., Liddicoat, M. I., … Upstill-Goddard, R. C. (2000). In situ evaluation of air-sea gas exchange parameterizations using novel conservative and volatile tracers. *Global Biogeochemical Cycles*, *14*, 373–387.

Parmentier, F.-J. W., Christensen, T. R., Sørensen, L. L., Rysgaard, S., McGuire, A. D., Miller, P. A., & Walker, D. A. (2013). The impact of lower sea-ice extent on Arctic greenhouse-gas exchange. *Nature Climate Change*, *3*(3), 195–202. https://doi.org/10.1038/nclimate1784

Prytherch, J., Brooks, I. M., Crill, P. M., Thornton, B. F., Salisbury, D. J., Tjernström, M., … Humborg, C. (2017). Direct determination of the air-sea CO2 gas transfer velocity in Arctic sea ice regions. *Geophysical Research Letters*, 2017GL073593. https://doi.org/10.1002/2017GL073593

Resio, D., Bratos, S., & Thompson, E. (2002). Meteorology and wave climate. *Coastal Engineering Manual, Part II, Hydrodynamics*, (1110–2), 1100.

Rutgers Van Der Loeff, M., Cassar, N., Nicolaus, M., Rabe, B., & Stimac, I. (2014). The influence of sea ice cover on air-sea gas exchange estimated with radon-222 profiles.

Journal of Geophysical Research - Oceans, *119*, 2735–2751. https://doi.org/10.1002/2013JC009321

Sahlée, E., Drennan, W. M., Potter, H., & Rebozo, M. A. (2012). Waves and air-sea fluxes from a drifting ASIS buoy during the Southern Ocean Gas Exchange experiment. *Journal of Geophysical Research: Oceans*, *117*(C8), C08003. https://doi.org/10.1029/2012JC008032

Shuiqing, L., & Dongliang, Z. (2016). Gas transfer velocity in the presence of wave breaking. *Tellus B: Chemical and Physical Meteorology*, *68*(1), 27034. https://doi.org/10.3402/tellusb.v68.27034

Smedsrud, L. H., Esau, I., Ingvaldsen, R. B., Eldevik, T., Haugan, P. M., Li, C., … Sorokina, S. A. (2013). The Role of the Barents Sea in the Arctic Climate System. *Reviews of Geophysics*, *51*(3), 415–449. https://doi.org/10.1002/rog.20017

Smith, M., & Thomson, J. (2016). Scaling observations of surface waves in the Beaufort Sea. *Elementa: Science of the Anthropocene*, *4*, 000097. https://doi.org/10.12952/journal.elementa.000097

Strong, C., & Rigor, I. G. (2013). Arctic marginal ice zone trending wider in summer and narrower in winter. *Geophysical Research Letters*, *40*(18), 4864–4868. https://doi.org/10.1002/grl.50928

Sutherland, P., & Melville, W. K. (2015). Field Measurements of Surface and Near-Surface Turbulence in the Presence of Breaking Waves. *Journal of Physical Oceanography*, *45*(4), 943–965. https://doi.org/10.1175/JPO-D-14-0133.1

Sweeney, C., Gloor, E., Jacobson, A. R., Key, R. M., McKinley, G., Sarmiento, J.-L., & Wanninkhof, R. (2007). Constraining global air-sea gas exchange for CO2 with recent

bomb 14C measurements. *Global Biogeochemical Cycles*, *21*. https://doi.org/10.1029/2006GB002784

Takahashi, T., Sutherland, S. C., Wanninkhof, R., Sweeney, C., Feely, R. A., Chipman, D. W., … de Baar, H. J. W. (2009). Climatological Mean and Decadal Change in Surface Ocean pCO_2, and Net Sea-air CO_2 Flux over the Global Oceans. *Deep-Sea Research Part II*, *56*, 554–577.

Terray, E. a., Donelan, M. a., Agrawal, Y. c., Drennan, W. m., Kahma, K. k., Williams, A. j., … Kitaigorodskii, S. a. (1996). Estimates of Kinetic Energy Dissipation under Breaking Waves. *Journal of Physical Oceanography*, *26*(5), 792–807. https://doi.org/10.1175/1520-0485(1996)026<0792:EOKEDU>2.0.CO;2

Tokoro, T., Kayanne, H., Watanabe, A., Nadaoka, K., Tamura, H., Nozaki, K., … Negishi, A. (2008). High gas-transfer velocity in coastal regions with high energy-dissipation rates. *Journal of Geophysical Research-Oceans*, *113*(C11), C11006. https://doi.org/10.1029/2007JC004528

Uhlig, C., & Loose, B. (2017). Using stable isotopes and gas concentrations for independent constraints on microbial methane oxidation at Arctic Ocean temperatures. *Limnology and Oceanography: Methods*, *15*(8), 737–751. https://doi.org/10.1002/lom3.10199

Upstill-Goddard, R. C., Wood, J., & Liddicoat, M. I. (1991). Sulphur hexafluoride and helium-3 as seawater tracers: Deployment techniques and continuous underway analysis for sulphur hexafluoride. *Analytica Chimica Acta*, *249*, 555–562.

Wåhlström, I., & Meier, H. E. M. (2014). A model sensitivity study for the sea–air exchange of methane in the Laptev Sea, Arctic Ocean. *Tellus B: Chemical and Physical Meteorology*, *66*(1), 24174. https://doi.org/10.3402/tellusb.v66.24174

Wanninkhof, R. (1992). Relationship between wind speed and gas exchange over the ocean. *Journal of Geophysical Research: Oceans*, *97*(C5), 7373–7382. https://doi.org/10.1029/92JC00188

Wanninkhof, R. (2014). Relationship between wind speed and gas exchange over the ocean revisited. *Limnology and Oceanography: Methods*, *12*(6), 351–362. https://doi.org/10.4319/lom.2014.12.351

Wanninkhof, R., Ledwell, J. R., Broecker, W. S., & Hamilton, M. (1987). Gas exchange on Mono Lake and Crowley Lake, California. *Journal of Geophysical Research: Oceans*, *92*(C13), 14567–14580. https://doi.org/10.1029/JC092iC13p14567

Wanninkhof, R., Asher, W. E., Ho, D. T., Sweeney, C., & McGillis, W. R. (2009). Advances in Quantifying Air-Sea Gas Exchange and Environmental Forcing. *Annual Review of Marine Science*, *1*. https://doi.org/10.1146/annurev.marine.010908.163742

Wanninkhof, R., Sullivan, K. F., & Top, Z. (2004). Air-sea gas transfer in the Southern Ocean. *Journal of Geophysical Research: Oceans*, *109*(C8), C08S19. https://doi.org/10.1029/2003JC001767

Woolf, D. K. (2005). Parametrization of gas transfer velocities and sea-state-dependent wave breaking. *Tellus B*, *57*(2), 87–94. https://doi.org/10.1111/j.1600-0889.2005.00139.x

Zappa, C. J., McGillis, W. R., Raymond, P. A., Edson, J. B., Hintsa, E. J., Zemmelink, H. J., … Ho, D. T. (2007). Environmental turbulent mixing controls on air-water gas exchange in marine and aquatic systems. *Geophysical Research Letters*, *34*. https://doi.org/10.1029/2006GL028790

Zappa, C. J., Raymond, P., Terray, E., & McGillis, W. R. (2003). Variation in surface turbulence and the gas transfer velocity over a tidal cycle in a micro-tidal estuary. *Estuaries*, *26*, 1401–1415.

Zappa, C. J., Ho, D. T., McGillis, W. R., Banner, M. L., Dacey, J. W. H., Bliven, L. F., … Nystuen, J. (2009). Rain-induced turbulence and air-sea gas transfer. *J. Geophys. Res.*, *114*. https://doi.org/10.1029/2008JC005008

Zhao, D., & Toba, Y. (2001). Dependence of Whitecap Coverage on Wind and Wind-Wave Properties. *Journal of Oceanography*, *57*(5), 603–616. https://doi.org/10.1023/A:1021215904955

Zhao, D., & Xie, L. (2010). A Practical bi-parameter formula of gas transfer velocity depending on wave states. *Journal of Oceanography*, *66*(5), 663–671. https://doi.org/10.1007/s10872-010-0054-4